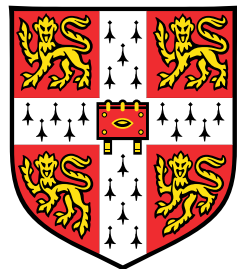


# Writing your PhD thesis in **L<sup>A</sup>T<sub>E</sub>X2e**

## Using the CUED template



**Krishna Kumar**

Department of Engineering  
University of Cambridge

This dissertation is submitted for the degree of  
*Doctor of Philosophy*

King's College

February 2017



I would like to dedicate this thesis to my loving parents ...



## **Declaration**

I hereby declare that except where specific reference is made to the work of others, the contents of this dissertation are original and have not been submitted in whole or in part for consideration for any other degree or qualification in this, or any other university. This dissertation is my own work and contains nothing which is the outcome of work done in collaboration with others, except as specified in the text and Acknowledgements. This dissertation contains fewer than 65,000 words including appendices, bibliography, footnotes, tables and equations and has fewer than 150 figures.

Krishna Kumar  
February 2017



## Acknowledgements

First and foremost, thanks to my supervisor Prof. Lee Thompson for his support over the last few years. Always happy to chat, even throughout those 16 months during which we were separated by six time zones, and always offering the ideal combination of advice and space, I am incredibly grateful to have had you as an advisor. Thanks also for the encouragement to make the most of all possible opportunities (and for always finding the money from somewhere!); I have really enjoyed working at Sheffield over the past few years.

I was privileged to spend nearly a year and a half of my Ph.D. out at Fermi National Accelerator Laboratory, near Chicago, IL, USA, and found it an incredible place to live and work. I'm not exaggerating when I say during my time there I would have happily never left! I am incredibly grateful to Dr. Michelle Stancari, Dr. Tom Junk and Dr. Tingjun Yang for giving me all the opportunities and being some of the most fun and productive people to work with – I consider myself extremely lucky to have had the opportunity to work closely with you all. I hugely enjoyed being a part of the 35-ton operations team and so must also thank Dr. Alan Hahn for his endless knowledge and conversation.

I would like to express my gratitude to the Science & Technology Facilities Council (STFC) for funding my Ph.D. and giving me the opportunity to travel and learn as much as I have. I am also hugely grateful to the Neutrino Division at Fermilab for paying my rent for almost a year, allowing me to stay at the lab for as long as I needed.

It's a constant source of relief that one doesn't go through this alone and I feel so lucky to have worked alongside some great friends, too numerous to mention. But to all those I have shared an office or a home with, at Sheffield and at Fermilab, and to those who started their Ph.D.s at the same time as me, thanks to you all for making the whole experience a fantastic one. Thanks also to those I shared American life with in Chicago, for everyone who lived in Fermilab Village at the same time as me, all forty-odd people who came to our house last Thanksgiving!, to the Social Soccer group and to everyone who would join me in my constant quest to spend as much as my life in Quigley's, or Sweet Potato Cafe, as possible, you all made me time out in the U.S. amazing and I'm grateful to all of you for the friendships.

Next, to all my friends from Southport and from Warwick for all the company, and for always going to the pub with me, over the last many years. You know who you all are and I'm thankful to each and every one of you!

Special thanks must be extended to my parents, and my brother, for their love and support throughout my entire life. I would never have got to the stage where I'm writing this mammoth document without the opportunities you have afforded to me, so I hope this thesis goes some way towards showing this gratitude!

Finally, last but certainly not least, to my amazing wife, Jenny. How you have put up with me, and all the physics, over the last eight years is beyond me but I'm constantly amazed by the level of love and support you show, and have shown right the way through my undergrad and Ph.D. Thanks for your continued patience throughout the years as we've been apart during my time in Warwick, Sheffield and Chicago. I wouldn't be where I am now without you and words cannot describe how much you have done for me (but if they could, they'd probably be in the form of this thesis!).

## **Abstract**

This is where you write your abstract ...



# Table of contents

<b>List of figures</b>	<b>xv</b>
<b>List of tables</b>	<b>xvii</b>
<b>1 Introduction</b>	<b>1</b>
1.1 Introduction to Neutrino Physics . . . . .	1
1.2 Current Understanding . . . . .	1
1.3 The Future . . . . .	1
<b>2 Neutrino Physics</b>	<b>3</b>
2.1 Neutrino Theory . . . . .	3
2.1.1 Neutrino Oscillations . . . . .	3
2.1.2 Neutrino Mass . . . . .	4
2.2 Future Neutrino Experiments . . . . .	4
2.3 The LAr TPC Concept . . . . .	4
2.3.1 A Brief History of Time (Projection Chambers) . . . . .	4
2.3.2 LAr TPC Operation . . . . .	6
<b>3 The DUNE Experiment</b>	<b>9</b>
<b>4 The DUNE 35 ton Prototype</b>	<b>11</b>
4.1 Motivation . . . . .	11
4.2 The Liquid Argon Purity Demonstrator . . . . .	12
4.2.1 LAPD Experimental Setup . . . . .	12
4.2.2 The LAPD Filtration System . . . . .	13
4.2.3 Purity Monitoring . . . . .	14
4.2.4 LAPD Results . . . . .	15
4.3 The 35 ton Cryostat . . . . .	16
4.3.1 Construction . . . . .	16

4.3.2	The 35 ton and LAPD . . . . .	16
4.4	The 35 ton Detector . . . . .	18
4.4.1	Detector Components . . . . .	18
4.4.2	Readout Electronics . . . . .	18
4.4.3	DAQ . . . . .	18
4.5	Filling the 35 ton . . . . .	18
4.6	The 35 ton Experimental Setup . . . . .	18
4.6.1	Filtration System . . . . .	18
4.6.2	Purity Monitoring . . . . .	19
4.7	35 ton Phase I . . . . .	19
4.7.1	Outcomes . . . . .	19
4.8	35 ton Phase II . . . . .	19
4.8.1	Commissioning . . . . .	19
4.8.2	The Sheffield Camera System . . . . .	19
4.8.3	Online Monitoring for Data Quality Monitoring . . . . .	19
4.8.4	Outcomes . . . . .	19
<b>5</b>	<b>Reconstruction in a Liquid Argon TPC</b>	<b>21</b>
<b>6</b>	<b>Online Monitoring and Event Displays for the 35 ton Experiment</b>	<b>23</b>
6.1	The DAQ Framework . . . . .	23
6.2	Online Monitoring Framework . . . . .	25
6.2.1	Monitoring Framework Design . . . . .	25
6.2.2	Writing Monitoring Data . . . . .	27
6.3	Data Quality Monitoring . . . . .	27
6.3.1	TPC Monitoring . . . . .	28
6.3.2	Photon Detector Monitoring . . . . .	28
6.3.3	External Counter Monitoring . . . . .	29
6.3.4	General Monitoring . . . . .	29
6.3.5	DQM Plots . . . . .	29
6.4	Online Event Display . . . . .	29
6.4.1	Selecting the Data . . . . .	31
6.4.2	Representing the Data . . . . .	33
6.5	Monitoring Web Interface . . . . .	34
6.5.1	Automated Data Transfer . . . . .	34
6.5.2	Web Page . . . . .	36
6.6	Online Monitoring Summary . . . . .	37

<b>7 Analysis of 35 ton Data</b>	<b>39</b>
7.1 Preparing 35 ton Data for Analysis . . . . .	39
7.1.1 Selecting the Data . . . . .	40
7.1.2 Improving Data Quality . . . . .	41
7.1.3 Reconstructing Muon Tracks . . . . .	41
7.2 Measuring LAr Purity from Crossing Muons . . . . .	44
7.3 APA-Crossing Muons . . . . .	44
7.3.1 T0 Determination from APA Crossing Tracks . . . . .	44
7.3.2 Charge Deposited by APA Crossing Tracks . . . . .	52
7.3.3 Comparison Between Drift Regions Using APA Crossing Tracks . .	56
7.4 APA Gap-Crossing Muons . . . . .	58
7.5 Shower Reconstruction in 35 ton Data . . . . .	58
<b>8 Electron Reconstruction for <math>\nu_e</math> Oscillation Signal at the DUNE Far Detector</b>	<b>59</b>
<b>9 Summary</b>	<b>61</b>
<b>References</b>	<b>63</b>
<b>Appendix A How to install L<sup>A</sup>T<sub>E</sub>X</b>	<b>65</b>
<b>Appendix B Installing the CUED class file</b>	<b>69</b>



# List of figures

2.1	Original TPC design, Nygren (1974) . . . . .	5
2.2	First LArTPC detector, Rubbia (1977) . . . . .	6
2.3	Affect of electric field on luminosity of ionisation electrons and scintillation light in a LArTPC . . . . .	8
4.1	LAPD tank and purification system . . . . .	13
4.2	Contaminant gradient in the LAPD tank . . . . .	14
4.3	Design of LAPD and 35 ton style purity monitors . . . . .	15
4.5	The 35 ton cryostat . . . . .	17
6.1	The <i>lbne-artdaq</i> framework . . . . .	24
6.2	Software framework built for 35 ton Online Monitoring . . . . .	26
6.3	Selection of Data Quality Monitoring figures . . . . .	30
6.4	35 ton data format . . . . .	32
6.5	Demonstration of how TPC data from a triggered event in a LArTPC is saved when employing a DAQ with continuous readout . . . . .	33
6.6	Example online event display made by the Online Monitoring framework . . . . .	35
6.7	Schematic showing the interface between the online monitoring system and the web . . . . .	36
6.8	Web page for online monitoring and event displays . . . . .	37
7.1	‘Good’ and ‘bad’ 35 ton runs . . . . .	40
7.2	Correcting for stuck codes in the 35 ton data . . . . .	41
7.3	Raw data stuck bit mitigation . . . . .	42
7.4	Coherent noise removal in 35 ton data . . . . .	42
7.5	Selecting tracks for 35 ton data analysis . . . . .	43
7.6	Event display showing the effect of unaccounting for T0 . . . . .	45
7.7	Method to align track segments on either side of the APAs involving minimising residuals from linear least square fit. . . . .	46

7.8	Method to align track segments on either side of the APAs involving minimising the distance between the projected intersection of each with the centre of the APAs. . . . .	46
7.9	Difference between the T0 calculated from TPC data and the T0 provided by the counters representing the trigger time of the through-going muon. . . . .	47
7.10	Correcting for T0 using $T_0^{\text{counter}}$ and $T_0^{\text{TPC}}$ . . . . .	47
7.11	Demonstration of the effect observed in the 35 ton data concerning tracks crossing the APAs. . . . .	48
7.12	Attempting to correct the track segment misalignment by assuming a misunderstanding of the spacing between the collection planes. . . . .	49
7.13	Attempting to correct the track segment misalignment by assuming a misunderstanding of the positioning of the collection wires inside the detector. . .	49
7.14	Attempting to correct the track segment misalignment by assuming an incorrect drift velocity. . . . .	50
7.15	Measuring the drift velocity of the ionisation electrons by taking tracks passing through opposite counter pairs and comparing the corresponding drift distance to the drift time. . . . .	51
7.16	The T0-corrected drift time for hits on APA crossing tracks. . . . .	52
7.17	The difference between the timestamps recorded by the PTB and the RCEs upon receiving a trigger. . . . .	53
7.18	. . . . .	53
7.19	The T0-corrected drift time for all hits on an APA crossing track in simulation. . . . .	54
7.20	Demonstration of the electron ionisation and hit collection for APA crossing tracks. . . . .	55
7.21	Comparison between the T0-corrected hit time distributions on APAs with and without the grounded mesh. . . . .	56
7.22	Comparison between the distribution of T0-corrected hit times for hits on wires in front of the APA frame and away from the APA frame to validate the functionality of the mesh. . . . .	57
7.23	Average lifetime-corrected charge per hit for hits on an APA crossing track separated according to whether or not the hit was collected around the interaction time. . . . .	57

# List of tables

2.1 Properties of noble elements relevant when considering a TPC medium for a neutrino experiment. . . . .	5
--	---



# **Chapter 1**

## **Introduction**

**1.1 Introduction to Neutrino Physics**

**1.2 Current Understanding**

**1.3 The Future**



# **Chapter 2**

## **Neutrino Physics**

Neutrino physics will be discussed!

- Theory
- Experiments
- Future Experiments

It may make sense to discuss the experiments as we go along...

I think the chapter will work best with both past, present and future woven together.  
And no distinct separation between theory and experiment (this is an experimental thesis after all...).

Can discuss the ‘neutrino problems’ to motivate the theory of neutrino oscillations, and include the SNO and Kamiokande results within.

Then something similar with mass.

And as we get onto unanswered questions, can weave the proposed experiments into this.  
I feel a section on the technology and concept of LAr TPCs will fit nicely into this setup.

### **2.1 Neutrino Theory**

#### **2.1.1 Neutrino Oscillations**

Derive 2-flavour case.

Extend to 3 flavour.

Discuss CP violation.

### 2.1.2 Neutrino Mass

Mass hierarchy.

Absolute mass.

## 2.2 Future Neutrino Experiments

## 2.3 The LAr TPC Concept

The use of a liquid argon time projection chamber (LArTPC) as a high-precision fine-grained detector medium holds much promise for the successful resolution of the open questions in neutrino physics. A great amount of R&D work has taken place to advance the maturity of the technology and pioneering experiments, such as ICARUS [1], have further increased the understanding of the neutrino community of the detector techniques. Past and currently running experiments at Fermilab, such as ArgoNeuT [], LArIAT [] and MicroBooNE [], are successfully using LArTPCs to take and analyse data and it seems certain to be the future of neutrino physics in the U.S.

This section will provide a brief history of LArTPC technology and motivate its potential when used in a huge experiment such as DUNE. The basic operation of such a detector will also be described to provide background for discussion of the DUNE and 35t experiments, and of reconstruction in LArTPCs, in future chapters.

### 2.3.1 A Brief History of Time (Projection Chambers)

The use of a time projection chamber as a potential particle detector was put forward by David Nygren in 1974 [3]. He envisioned bubble-chamber quality data but with the possibility of digital readout of the data, facilitating extremely fine spatial resolution, good timing resolution and fast recovery after triggering. The basic concept is a drift chamber containing a noble gas placed within a field to drift ionisation electrons created by a propagating particle towards a multielectron array. This setup allows full three-dimensional reconstruction by combining information from the two-dimensional readout plane with the drift time. Nygren also included a magnetic field to assist particle identification in his design, shown in Fig. 2.1.

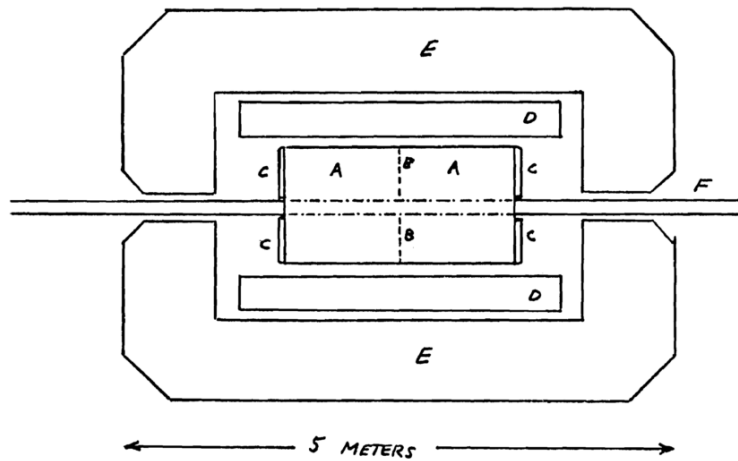


Fig. 2.1 The original concept of the time projection chamber particle detector, drawn by David Nygren in 1974 [3].

The extension of this concept to a liquid argon TPC and its potential as a high-precision fine-grained detector medium in neutrino physics was proposed by Carlo Rubbia in 1977 [4]. The use of a noble liquid rather than gas is necessary in neutrino experiments to provide a high enough target mass to increase the probability of a neutrino interaction. Noble liquids have high electron mobility and low diffusion, favourable properties as the detection of particles is from the ionisation and scintillation light created by the particles. Given the necessity of a high electric field in order to drift these electrons to the readout places, excellent dielectric properties are also required; noble liquids possess such qualities. The properties of liquid argon which make it almost perfect for this use are demonstrated in the table in Table 2.1.

Table 2.1 Properties of noble elements relevant when considering a TPC medium for a neutrino experiment.

	Water	He	Ne	Ar	Kr	Xe
Boiling point [K] @ 1 atm	373	4.2	27.1	87.3	120.0	165.0
Density [g/cm <sup>3</sup> ]	1	0.125	1.2	1.4	2.4	3.0
Radiation length [cm]	36.1	755.2	24.0	14.0	4.9	2.8
Scintillation [ $\gamma$ /MeV]	-	19 000	30 000	40 000	25 000	42 000
dE/dx [MeV/cm]	1.9		1.4	2.1	3.0	3.8
Scintillation $\lambda$ [nm]		80	78	128	150	175
Natural abundance (Earth atm) [ppm]		5.2	18.2	9340.0	1.10	0.09
Electron mobility [cm <sup>2</sup> /Vs]		low	low	400	1200	2200

An additional advantage of this technology is the low threshold for detection; this is set by the ionisation threshold of liquid argon and is only  $23.6 \pm 0.5$  eV [4]. Rubbia realised that a LArTPC could be the digital replacement for the high quality particle detection methods used in bubble chambers, very common in neutrino physics in the 1970s. He proposed the first LArTPC detector design, shown in Fig. 2.2, which bears a striking resemblance to the LArTPC used in experiments today.

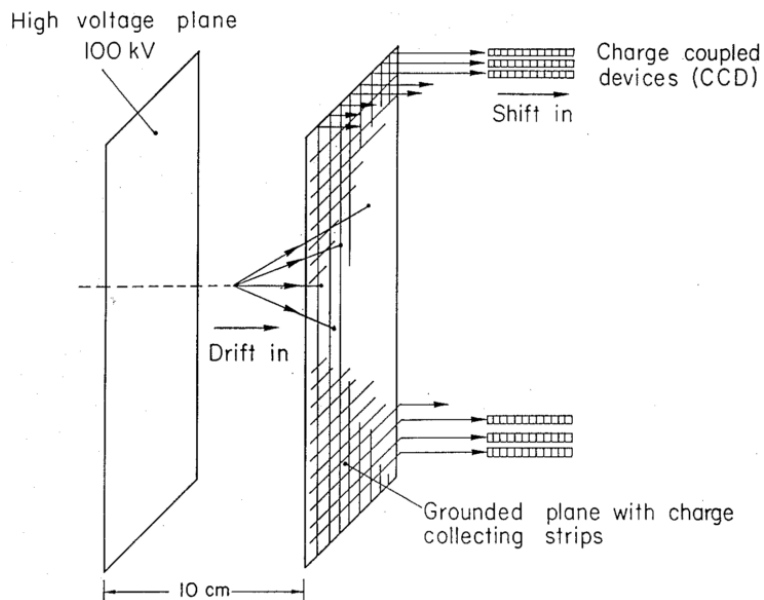


Fig. 2.2 The LArTPC detector proposed by Carlo Rubbia in 1977 [4].

Constructing and operating such a detector was beyond the technology of the time, and is still being understood today. The operation of a LArTPC detector and the challenges associated with this are the subject of section 2.3.2.

### 2.3.2 LAr TPC Operation

explain how they work

new subsubsection

[FIND OR MAKE A FIGURE TO GO WITH THE FOLLOWING DESCRIPTION...]

A LArTPC typically consists of a single, or multiple anode and cathode, at either end of an active drift region. An ionising particle passing through a LArTPC causes electrons to become free from argon atoms and, in the presence of a field, drift towards an anode where they are read out.

The readout consists of multiple wires planes with different orientations to facilitate the reconstruction. The wires are either ‘induction’ wires, which allow the electrons to deposit

charge but continue past, or ‘collection’ wires, on which the electric field lines end and all the charge on the electron is collected. Each wire plane is therefore held at a different ‘bias voltage’ to prevent any field lines ending on the induction wire, thus creating local electric fields which promote the continuing forward motion of the electrons. The signal seen is therefore dependent on the type of wire plane; a bipolar pulse on an induction plane wire and unipolar on a collection plane wire. It is also common, though not essential, to make use of a ‘grid plane’ upstream of the signal planes in order to shield them from the electron charge until they are close. Without such a plane, the bipolar pulse would be highly asymmetric, though would still have zero integral. It also makes changing the drift voltage (controlling the electric field) slightly easier as the signal planes are somewhat shielded from its effects. MicroBooNE does not operate with a grid plane and, although the 35t and the DUNE reference design make use of a grid plane, it is uncertain whether the benefit outweighs the cost for a huge LArTPC detector such as the DUNE far detector. It is worth mentioning alternative readout possibilities have been suggested but, given the scale of future LArTPCs, it is highly unlikely a viable solution which delivers superior readout at a comparable cost will be found.

Given the positive ions that are left in the medium, there is the possibility of recombination at a later time and therefore a loss of information about the initial interaction.

This is however accompanied by a flash of scintillation light which is hugely useful as a means of determining the event ‘start time’ ( $t_0$ ); without this information it would be impossible to place an absolute time scale on the interaction and we would therefore not be able to resolve the coordinate along the drift direction. The magnitude of the electric field applied is the key to both processes and there is thus a compromise which must be struck in order to preserve as much information as possible. The graph in Fig. ?? demonstrates this; a field of 500 V/cm is often chosen in current LAr neutrino experiments.

A cathode is held at a high voltage

Flesh this stuff out...

U plane, V plane and collection all held at different fields. Slightly increasing in order to promote forward motion of the electrons. V held at 0V because it’s cheaper (don’t need crazy voltages, just some negative (still quite high, 100V), 0V and some positive. Grid plane (also held at potential) is to shield the APAs from the electrons until they are close. Not needed, but if not present then pulse wouldn’t be very bipolar! The charge in both portions will still equate but the leading end will be muchhhh longer. All electric field lines (generated from movement of electrons) end on the cathode; don’t want them to end on the induction wires (hence making sure the field increases). We want them to end on the collection planes, which collects the charge. Signal shaping time (along with gain, the two front-end ASIC

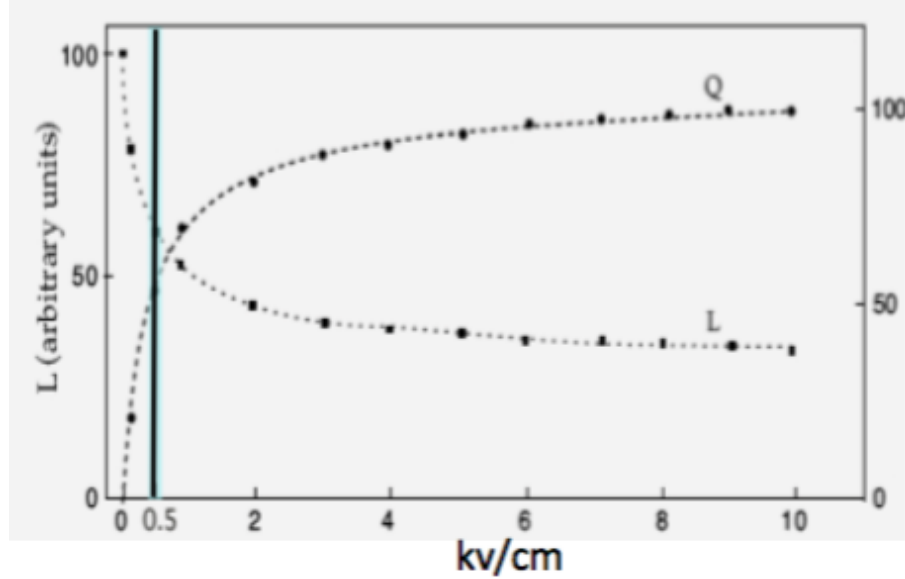


Fig. 2.3 Demonstration of the competing effect the electric field has on the luminosity of the ionisation electrons and scintillation light arriving at the detector readout. Since both are essential in reconstructing the complete interactions, a balance must be found. [PLACEHOLDER IMAGE].

parameters) is to let the charge leave the wire before being hit again (or something like this!). Deconvolution I still need to understand...

In 35t, we have FE ASICs which are the very front end and apply the signal shaping and gain. Have regulators to control the power these receive (these are noisy...). Also ADC ASICs to do digitisation in the cold. MicroBooNE don't do this, this just have the front end and do everything else in the warm. FE ASICs are the problem, same for uBooNE and 35t. ADC ASIC has stuck code problem.

# **Chapter 3**

## **The DUNE Experiment**



# **Chapter 4**

## **The DUNE 35 ton Prototype**

The 35 ton is a prototype experiment for the DUNE far detector design. It was constructed to prototype the unique design features of the LBNE far detector and was the only planned prototype for this detector. Following the dissolution of LBNE and the subsequent merging along with LBNO into the DUNE experiment, the 35 ton has become an integral part of the design and execution of the DUNE far detector design.

The 35 ton consists of a membrane cryostat (Sec. 4.3), designed to be filled with 35 metric tons of liquid argon, and a small-scale DUNE-style detector (Sec. 4.4) including a TPC and photon detectors. It was constructed in 2012 at PC4, a former proton facility in a decommissioned beamline, at Fermilab. The Phase I run, without a detector, took place between December 2013 and February 2014. Between February 2014 and September 2015 the detector was constructed and heavily tested at FNAL before being installed inside the cryostat ready for the Phase II run. This took place between February 2016 and April 2016 (officially starting on 11th February, as I type!).

### **4.1 Motivation**

The use of liquid argon TPCs (LArTPCs) for the study of neutrinos in long-baseline experiments shows great promise and is the direction neutrino research, particularly in the US, is headed. Fermilab has an extensive program of LArTPC experiments to design, test and improve such detectors, culminating in DUNE, the flagship experiment due to come online in the early 2020s. Although they exhibit great physics potential, they do not come without significant engineering challenges. For example, DUNE will have four 10 kton cryostats containing liquid argon kept at very high purity. Constructing such a cryostat is itself difficult and expensive but in order to achieve, and maintain, the required purity, much R&D is required.

Previous LArTPC experiments, such as ICARUS [], Argoneut [], LArIAT [] and MicroBooNE [] (?), have been constructed as flat plane vessels and have used an evacuation method as the first step in removing atmospheric impurities which would contaminate the liquid argon. Constructing the DUNE far detector cryostats in a similar manner would be both very expensive and incredibly challenging. In order to investigate possible alternatives, the Fermilab program includes the Liquid Argon Purity Demonstrator (LAPD) and 35 ton experiments, together showing a cheaper and more feasible approach to designing and operating LArTPCs. These experiments are the subject of the present chapter.

## 4.2 The Liquid Argon Purity Demonstrator

The Liquid Argon Purity Demonstrator (LAPD) [5] was designed to demonstrate that the required purity of future LArTPC experiments is possible to achieve without the use of large scale vacuum pumps. The required mechanical capability of the cryostat to withstand such a method, along with the operation of the evacuation system itself, adds a considerable amount to the cost of the project. Suggestions to get around this include using multiple smaller scale cryostats, but this leads to greater complexity relating to both the engineering requirements of the piping infrastructure and the reconstruction capabilities of interactions spanning numerous fiducial volumes. LAPD successfully pioneered the method of using purging as the first step in purification of the liquid argon. This important result is discussed below and has significantly influenced the design of future LAr cryostats, including the 35 ton.

### 4.2.1 LAPD Experimental Setup

LAPD consists of a cylindrical tank (diameter 10 feet, height 10 feet) with a domed head capable of holding 32.6 tons of liquid argon. It is instrumented with cryogenic equipment and a purification system, consisting of two purifiers and a piping system. Figure ?? shows a CAD model of the tank and purification piping.

Insulation for the tank is provided by fibreglass sheets covering the outer volume which, along with the tank, is refrigerated by liquid nitrogen from an external supply. There also exist cooling coils near the top of the tank which serve to recondense vapourised argon and feed it back into the tank, via the filtration system.

The liquid argon is fed into the tank from outside PC4. The argon purity is maintained through the use of the purifiers, located outside of the main volume. Argon is constantly circulated from the tank to these vessels through stainless steel pipes. The filtration system

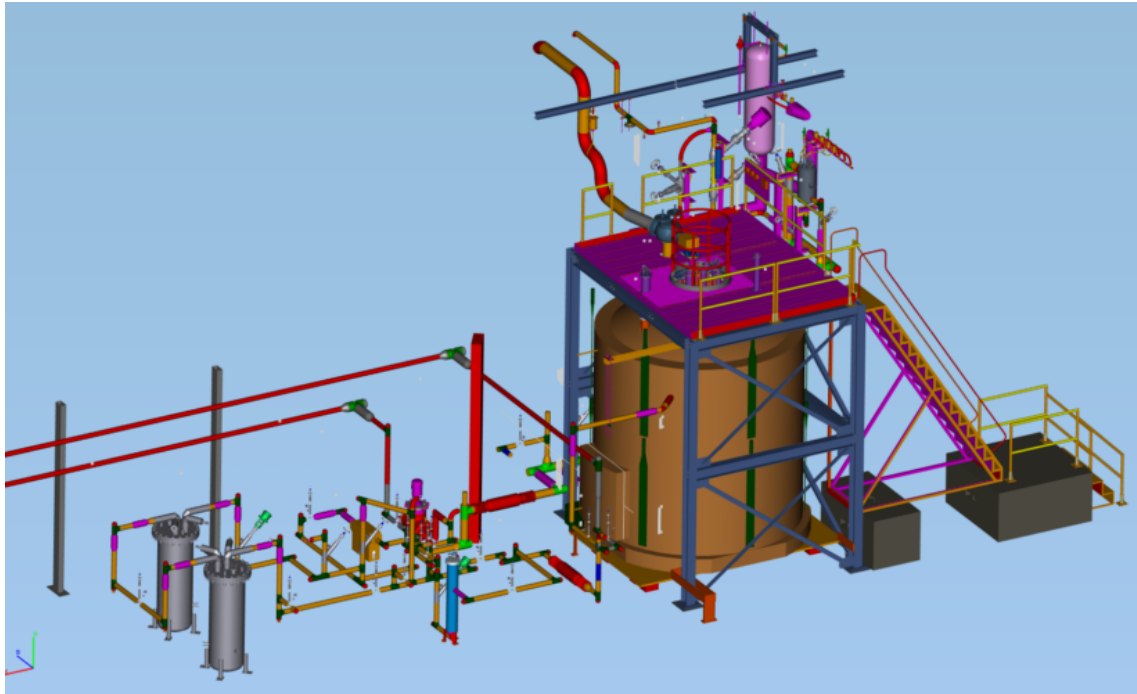


Fig. 4.1 The LAPD tank and purification system [5]. The domed tank on the right, beneath the platform, is the cryostat. The piping allow the flow of liquid argon into and out of the cryostat and is used as part of the purification system. Two cylindrical purifiers, visible in the lower left of the figure, remove contaminants from the argon as it is pumped through. All components of the experiment are discussed in the text.

used by LAPD, and subsequently by the 35 ton cryostat, is discussed in greater detail in section 4.2.2.

### 4.2.2 The LAPD Filtration System

A LArTPC relies on the detection of the drift electrons produced upon ionisation of the argon by a propagating particle. Electronegative contaminants in the medium jeopardise this process by recombining with the electrons before they can reach the readout electronics. The phase ‘electron lifetime’ therefore refers to the amount of time that an electron will typically drift along the electron field, and is directly related to the concentration of impurities in the liquid. Even using a modularised detector, as the DUNE far detector will be, drift lengths on the order of 5 m are realistically required, leading to purity requirements of several milliseconds. The dominant contaminants which are removed by the LAPD and 35 ton filtration system are oxygen and water.

The liquid argon is extracted from near the bottom of the tank and returned to the top after passing through the purifiers. It first passes through the water filter before continuing

on through the oxygen filter. The water filter comprises a molecular sieve which prevents the propagation of large molecules, such as water. This purification step must occur first since the proceeding filter also removes water molecules and would therefore be less efficient at removing oxygen if used first. The oxygen filter consists of a thin activated-copper layer on an alumnia substrate [2]. Both filters will lose some functionality over time as they collect more and more impurities and so require ‘regenerating’ in order to remove the contaminants. This can be done in-situ, as described in [2]; this complicates the design of the filter but is necessary when considering the purification system required for the full DUNE far detector.

The contamination gradient, and associated purities at each stage during the LAPD Phase II run, is shown in figure 4.2. These purities are known through the use of purity monitors; these are the subject of section 4.2.3.

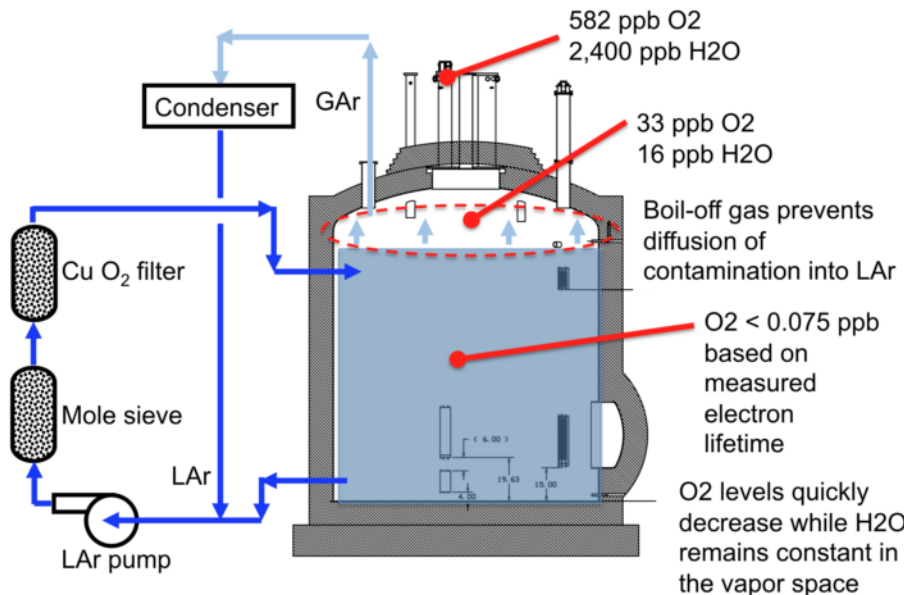


Fig. 4.2 Contaminant gradient in the LAPD tank at different stages of the purification process [5]. The associated LAr purities, in units of parts-per-billion (ppb) are also shown.

### 4.2.3 Purity Monitoring

As discussed in section 4.2.2, extreme LAr purity is required for the successful readout of ionisation electrons by the electronics. These purities must be constantly monitored to ensure the high quality of argon necessary during data taking. Since these impurity concentrations are beyond the capabilities of many conventional gas analysers, a device called a purity monitor is employed. Such a device is shown schematically in figure 4.3.

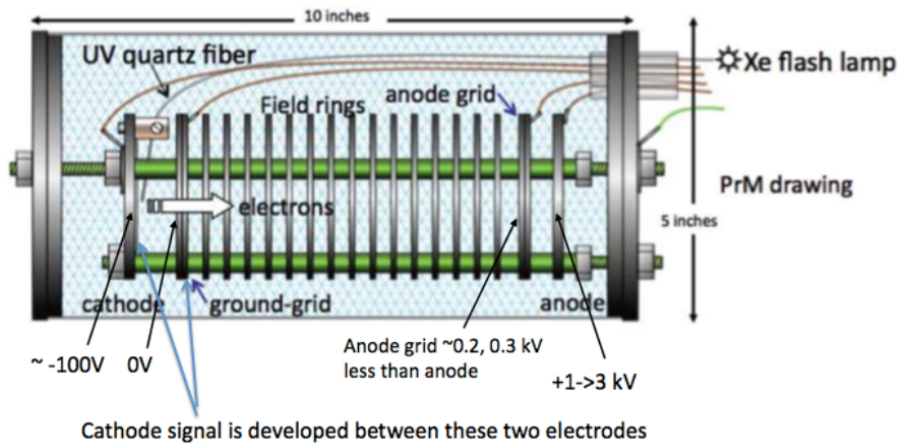


Fig. 4.3 Diagram showing schematically the design of purity monitor used in LAPD, and subsequently the 35 ton experiment [? ]. Their use is described in the text.

The purity monitors deployed consist of a cylindrical volume, filled with LAr for its surrounding environment. They contain a photo cathode and an anode, between which lies short drift volume. When taking purity measurements, light from a Xenon flash lamp is incident on the cathode, liberating photoelectrons which traverse towards the anode. Electronegative impurities in the LAr will decrease the electron lifetime and therefore the mean number of electrons reaching a certain point along the drift volume. A measurement of the ratio of the charge arriving at the anode to that at the cathode is hence a measurement of the inherent purity of the liquid.

These monitors were placed both in the LAPD tank and just after the filtration system in order to study the purity at different points in the recirculation. Several gas analysers, measuring nitrogen, oxygen and water contaminants to various levels of accuracy, were also used. Temperature sensors to measure the vertical temperature profile within the cryostat were necessary to account its effect on the electron drift velocity.

Several of the technologies pioneered in LAPD were also used in the 35 ton experiment, as will be shortly discussed.

#### 4.2.4 LAPD Results

LAPD successfully demonstrated achieving and maintaining the required LAr purity for a large neutrino detector is possible without the costly and challenging use of evacuation techniques. It initially ran for six weeks and reached a purity of better than 60 ppt (parts-per-trillion) oxygen equivalent [5]. The measured electron lifetimes over the course of the run is

shown in figure ???. As can be seen, electron lifetimes of up to 4 ms were reached, which is [put into context with current DUNE requirements!].

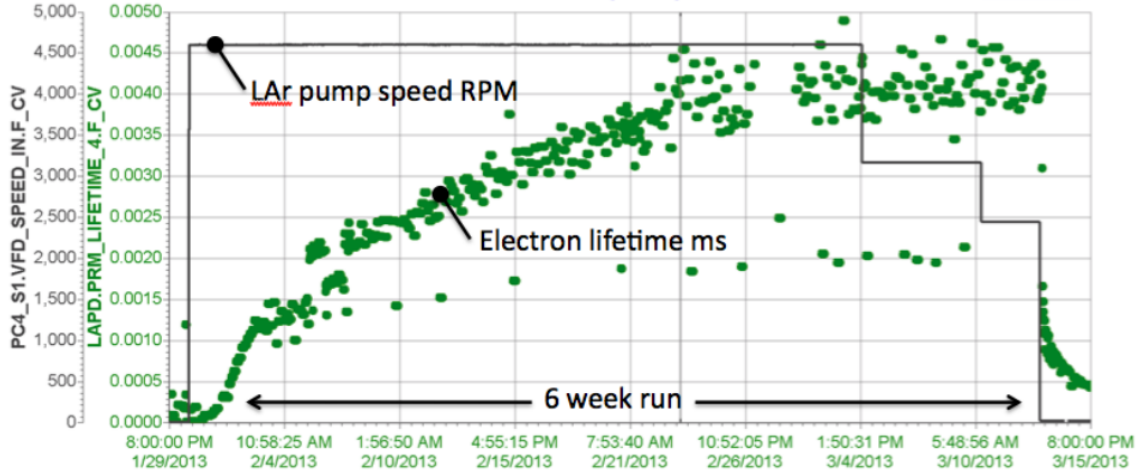


Fig. 4.4

This important result has great significance when considering future LArTPC experiments and laid the way for the 35 ton experiment. This experiment will now be discussed in the subsequent sections.

## 4.3 The 35 ton Cryostat

The 35 ton prototype takes advantage of membrane cryostat technology and is the first test of this construction technique for LArTPCs. Membrane cryostats have been widely used in the liquified natural gas industry for many years but the 35 ton experiment is the first to make use of the technology for liquid argon. Furthermore, it is the first membrane cryostat to be constructed in the United States and the first to be constructed for scientific purposes [? ]. The 35 ton cryostat is the subject of the present section.

### 4.3.1 Construction

Boring stuff about cement and shit.

Cryostat!

### 4.3.2 The 35 ton and LAPD

It's near LAPD!

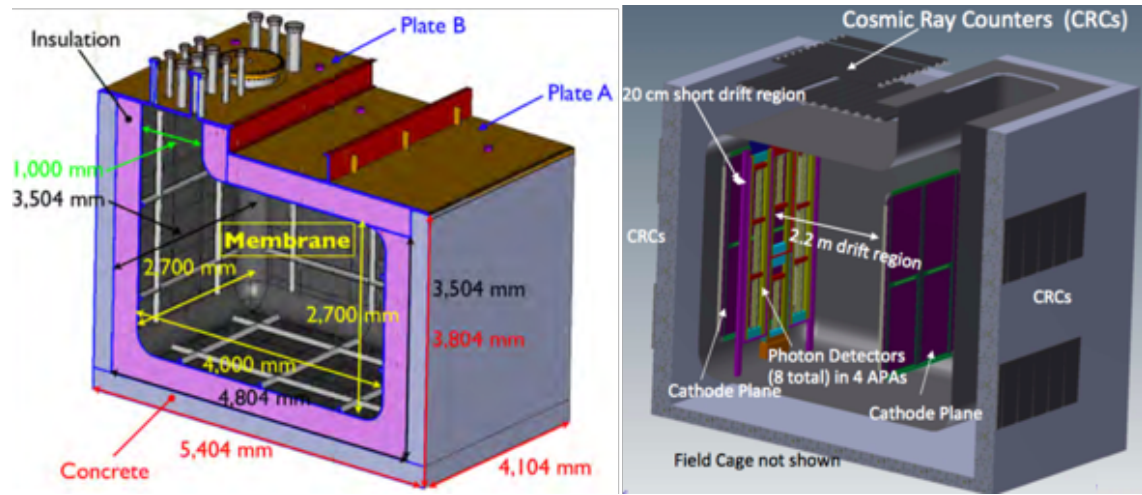


Fig. 4.5 The 35 ton cryostat [? ]. The cryostat as operated during Phase I is shown on the left and the corresponding version, including a full small-scale detector, used in Phase II is on the right.

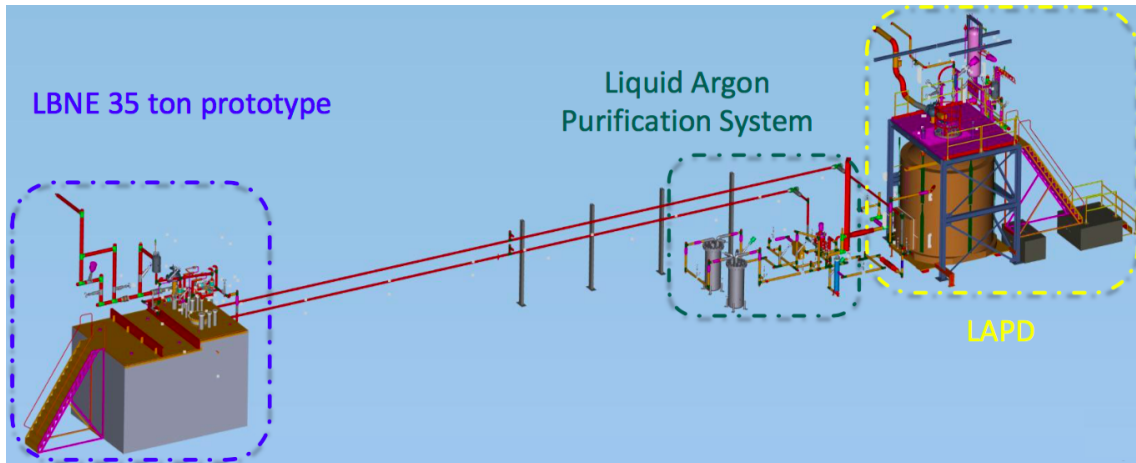


Fig. 4.6 [? ].

## 4.4 The 35 ton Detector

### 4.4.1 Detector Components

#### 4.4.1.1 TPC

#### 4.4.1.2 Photon Detectors

#### 4.4.1.3 External Counters

### 4.4.2 Readout Electronics

#### 4.4.2.1 FEMBs

#### 4.4.2.2 RCEs

#### 4.4.2.3 SSPs

#### 4.4.2.4 PTB

### 4.4.3 DAQ

## 4.5 Filling the 35 ton

## 4.6 The 35 ton Experimental Setup

### 4.6.1 Filtration System

Same as LAPD.

### **4.6.2 Purity Monitoring**

Same as LAPD.

## **4.7 35 ton Phase I**

### **4.7.1 Outcomes**

## **4.8 35 ton Phase II**

### **4.8.1 Commissioning**

### **4.8.2 The Sheffield Camera System**

Wait for Nicola to finish the paper and plagerise!

### **4.8.3 Online Monitoring for Data Quality Monitoring**

### **4.8.4 Outcomes**



# **Chapter 5**

## **Reconstruction in a Liquid Argon TPC**



# Chapter 6

## Online Monitoring and Event Displays for the 35 ton Experiment

Monitoring of the data collected during the running of an experiment is imperative to ensure a high quality of data is maintained. Such monitoring is often provided in real-time ('Online Monitoring'), summarising the data from the current run, or in near real-time ('Nearline Monitoring'), summarising data over runs from typically the previous day, week or month to represent the longer term fluctuations in the data quality. The system developed to provide online feedback for the 35 ton Run II data taking period is discussed in this present section.

An event display, designed to illustrate physics events as they occur in the detector, is another desirable feature that is particularly useful during data collection. A basic example of such a display is also produced by the monitoring system for the purposes of ensuring good quality physics data collection is maintained.

The system is designed to be flexible and provide prompt feedback for those operating the experiment. It was thus included as part of the DAQ (Data Acquisition) system, *lbne-artdaq*, discussed in Section 6.1. The monitoring framework itself is the subject of Section 6.2, with its two functions, data quality monitoring and producing online event displays, presented in Section 6.3 and Section 6.4 respectively. Finally, the web interface developed to allow synchronisation of this monitoring data to a dedicated web page for ease of access is briefly described in Section 6.5.

### 6.1 The DAQ Framework

Experiments at FNAL are migrating to *artdaq*, a centrally-maintained data acquisition system built on the art framework utilised by all offline software written for experiments hosted at

the lab. The DUNE 35 ton experiment was one of the first to use this new software (only LArIAT had previously used it for data taking) and used an experiment specific system named lbne-artdaq. A general overview of lbne-artdaq is shown in Figure 6.1.

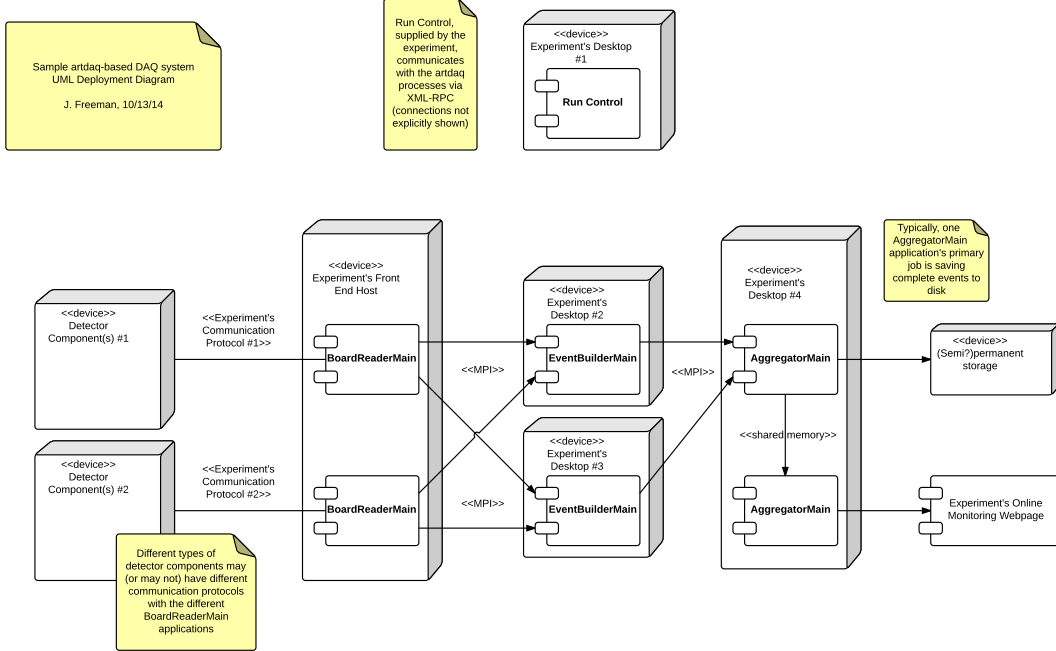


Fig. 6.1 Overview of the *lbne-artdaq* framework used for data acquisition by the DUNE 35 ton experiment. See the text for a complete description. [Thank John Freeman for this image... how to reference?]

Data flows from left to right and pass through components common to most DAQ systems. Closest to the detector components (i.e. the RCEs, SSPs and PTB [see Section ??]) are the board readers which take the output from the firmware as soon as it is ready and sends it downstream to the event builders. There exists a board reader for each of the detector components (totalling 24) and each is unaware of the existence of the others. It is the job of the event builders to assemble a full ‘event’ from these individual ‘fragments’ passed on from each of the detector elements. An event is complete once composed of a full set of fragments and the event builders will wait to receive them all before sending the data onwards to the aggregators.

There are two aggregators which take the full events but process them in very different ways. All the data passes through only the first aggregator, whose function it is to write the output to disk and thus end processing by the DAQ. The second aggregator receives no events

but instead has access to the shared memory occupied by the data as it passes through the first aggregator; it is thus designed specifically for the purpose of monitoring and in no way affects the data or the output from the first aggregator. It is within this second aggregator process that the online monitoring system described in the proceeding section is designed to run.

Each of the DAQ processes runs on a machine on the private DAQ network and is configured as normal within art (using the *fhicl* (Fermilab Hierarchical Configuration Language) configuration language). Two nodes on the main FNAL network (lbne-gateway01/02) provide access to these private machines, of which there are 7 (lbnedaq1-7), and contain all scripts and setup necessary to run through the DAQ via a command line interface.

## 6.2 Online Monitoring Framework

The framework developed for the monitoring system had the following design goals:

- to be able to analyse the data read out of memory in its raw ‘DAQ format’;
- to be as computationally efficient as possible to allow for processing at the event rate (data taking rate);
- to provide the flexibility for further monitoring plots to be added with ease;
- to allow for use of an online event display to provide comprehensible images of the raw data.

In general, the final developed system succeeded in all these goals and provided invaluable information, becoming an integral tool in the commissioning and the data taking of the 35 ton. An illustration of the framework is shown in figure 6.2.

### 6.2.1 Monitoring Framework Design

The setup consists of a central ‘module’, `OnlineMonitoring_module.cc`, which is configured within the art framework through its base class. The `OnlineMonitoring` class controls the running of the system and owns instances of further classes, each designed for a specific purpose, controlling the data flow by calling the relevant methods when required. Once an event has been obtained, the data for each component is processed and repackaged into `RCEFormatter`, `SSPFormatter` and `PTBFormatter` objects. The purposes of this method are thus:

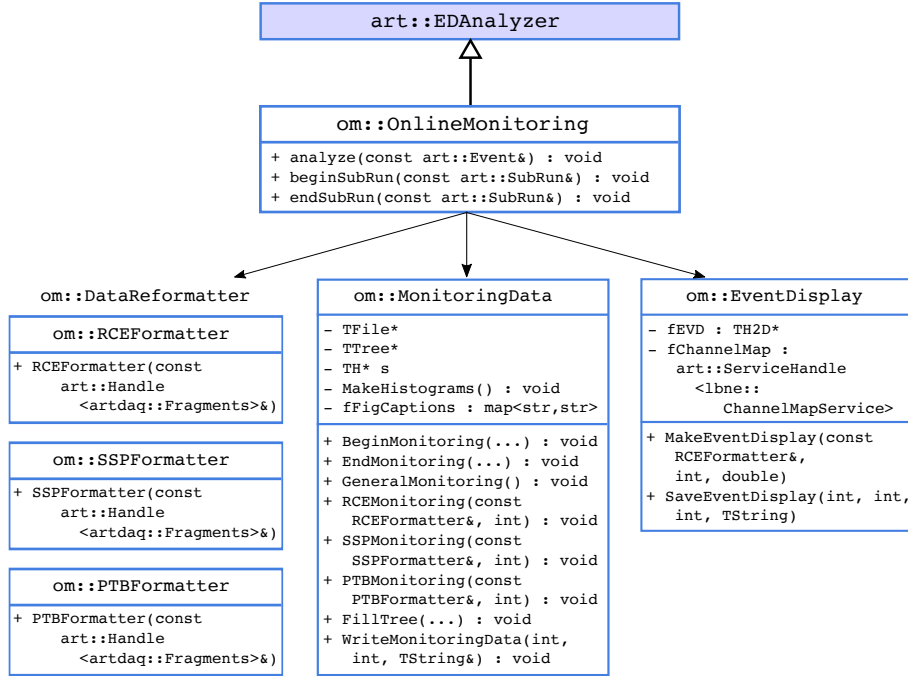


Fig. 6.2 Demonstration of the framework designed for online monitoring in the DUNE 35 ton experiment.

- to provide an interface between the raw data and the methods which analyse the data. This is important as it provides a single point of maintenance for when formats change and allow for various ‘DAQ modes’ to use the same analysis code;
- to separate interaction with the DAQ from the handling of output data objects;
- to facilitate random access of the data for more detailed analysis which would not be possible if just processing linearly.

The main drawback to performing this step is it requires all the data to be held in memory until the end of the event and represents basically the same information as initially present. However, it was decided the advantages were worth the compromises in memory usage required and no problems were apparent during the course of the run except when operating at the very limits of the capability of the DAQ.

These reformatted data objects are then passed to the methods in the `MonitoringData` class for straight-forward analysis. This class owns all of the data products which are output from the monitoring (e.g. histograms, graphs, trees and files) and deals with their filling and writing out when required. This is discussed further in Section 6.3.

The event display is handled by its own dedicated class, `EventDisplay`; this has methods for making the displays and saving them as an image in the correct place when required. It is

designed to accept the reformatted RCE object and presents the data in as meaningful way as possible; this is detailed fully in Section 6.4.

### 6.2.2 Writing Monitoring Data

The data objects are created new for each subrun and are written out at three points during data taking:

- an initial write out N seconds after the start of the subrun;
- at frequent intervals during the subrun, every M seconds;
- at the end of the subrun.

The parameters N and M are user defined and were set to 30 and 500 respectively for normal data taking. The data products are only cleared at the end of a subrun, so any intermediate writing out of data simply refreshes the current plots.

The event displays are computationally expensive to make and so were only created once per subrun during normal running. However, since a subrun was automatically stopped by the DAQ and a new one started once the output file had reached 5 GB in size, and (since zero suppression was not utilised at any point during the run) this occurred on average every four minutes, a new event display was made every few minutes.

All the output data are saved on a shared disk on the gateway DAQ machines for further use. This is discussed in Section 6.5 below.

## 6.3 Data Quality Monitoring

The overarching aims of the online monitoring system was to provide direct feedback informing the operators of the quality of the data being taken. This is vital for various different aspects of data taking, for example

- ensuring all detector components being used in the current run are receiving and processing data;
- noting the TPC readout has entered the ‘high noise state’ and acting accordingly; [MW: I will probably have explained what this is in a previous chapter!]
- checking the trigger rates from the external cosmic muon counters are feasible.

The monitoring was diagonalised in a similar way to the DAQ readout with data from the TPC, photon detector and external counters processed separately.

### 6.3.1 TPC Monitoring

Ensuring the high quality of TPC data involved mainly considering various distributions of the ADC values provided by the front-end boards, separated by channel, board and APA. The mean and RMS of the ADC values for a given channel provides information such as the measured pedestal and the level of noise being read out. The uncorrelated component of the noise can be monitored using the concept of ‘DNoise’; this considers the difference in ADC value between two neighbouring channels at a given readout time and represents the level of noise which would be impossible to remove by the use of coherent noise filters only. Unfortunately, for the 35 ton, this uncorrelated component made up most of the noise across all channels (see Figure 6.3a). FFTs of the signal waveforms, performed separately for each RCE, were also useful in monitoring bands of noise in frequency space.

Monitoring of various other problems, such as the ‘digitiser stuck code’ issue, synchronisation concerns resulting in a different number of microslices being saved in corresponding RCE millislices, and the asymmetry of bipolar pulses, were added as these issues became apparent during the commissioning.

### 6.3.2 Photon Detector Monitoring

Analogously to the TPC situation, monitoring of the photon detectors mainly involved considering various ADC distributions separated by optical channel and by detector. The peak height, pedestal and integral of each waveform were also considered as a function of channel to ensure each were operating consistently.

The triggers sent on by the SSPs were also studied; unfortunately due to the design of the monitoring framework (with it not guaranteed to receive each event), trigger rates were challenging to compute. Eventually, it was decided to leave them in the monitoring but only consider the relative rates – the monitoring code was used offline, processing closed files, to ensure all events were considered and determine accurate rates. Along with the trigger rate, the number of triggers, the fraction of events containing a trigger and the number of readout ticks within each trigger were also considered.

During installation, one photon detector was erroneously left unconnected to its SSP and so was unavailable during the run. This was discovered using the online monitoring – unfortunately after the cryostat had been sealed however.

### 6.3.3 External Counter Monitoring

Since monitoring the external counters primarily involves considering trigger rates, a similar problem to that encountered in the photon detector monitoring was faced. A similar solution was agreed upon and the trigger rates were only considered relative to different counters. For each counter, the hit rate and the average activation time were monitored to ensure counters in similar positions were recording similar cosmic muon data. The number and type of payloads sent on from the PTB were also detailed so the amount of data, along with information about what the data are comprised of, can be monitored.

### 6.3.4 General Monitoring

A variety of useful quantities not pertaining to any specific subcomponent were also monitored to assure smooth data taking. These include the size of output files from recent runs, the average event size from recent runs, information about which detector subcomponents are taking data and the number of events seen by each and also synchronisation information between various detector components.

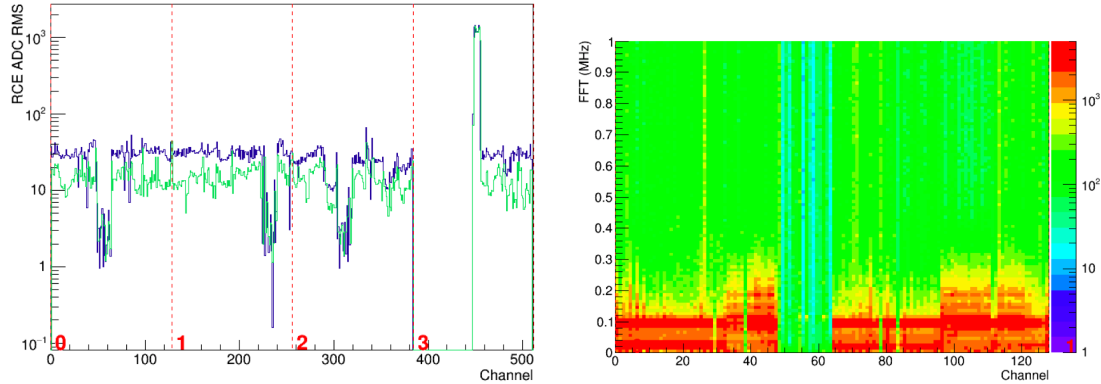
### 6.3.5 DQM Plots

The DQM section of the online monitoring produced around 60 figures each time it is run, illustrating the data discussed in the previous sections. It is unnecessary to reproduce many here [perhaps an appendix? I think unnecessary though] but a sample for reference are shown in Figure 6.3.

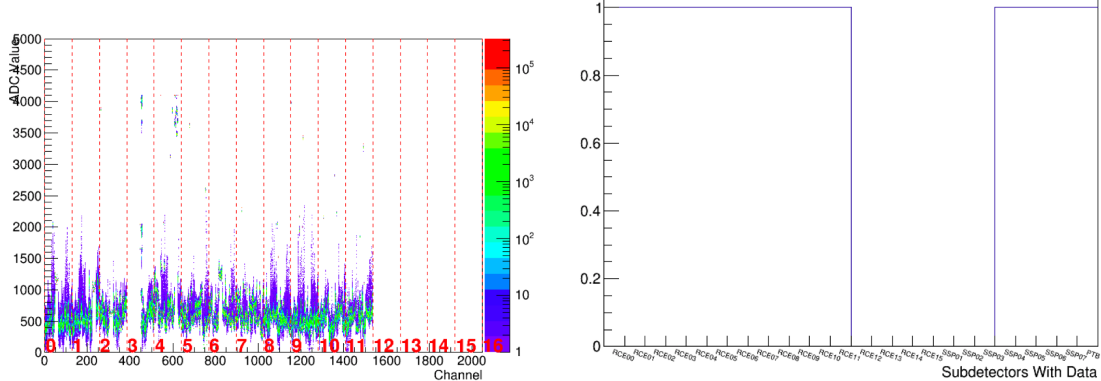
## 6.4 Online Event Display

One of the highlights of being in ROC West (Remote Operation Control room at FNAL) during data taking was watching the online event display refresh with updated images representing cosmics passing through the detector. The event display additionally allowed for straight-forward monitoring of the data – high noise states, poor LAr purity and drift field problems were all immediately evident from the display.

Given the way in which data were read out of the detector, it proved challenging finding a way to represent this in a simple way that was comprehensible. The construction of such a display is the subject of this section.



(a) TPC noise. The total noise (RMS of the ADC (b) FFT of the waveform read out by the first values) is shown in blue and the uncorrelated RCE (channels 1–128). component of this noise is shown in green. This is determined by considering the ‘DNoise’, the difference in ADC between neighbouring channels for any given tick.



(c) ADC values as a function of channel; incredibly useful plot containing the mean and RMS for all channels together. (d) Subdetectors which are successfully collecting data. In this particular run, it can be seen one quarter of the TPC readout was turned off, along with three photon detector readouts.

Fig. 6.3 Demonstration of various plots used in the Data Quality Monitoring for the 35 ton. [Images are probably placeholders at the moment and should be reconsidered.]

### 6.4.1 Selecting the Data

[The data format will likely be described in the 35 ton section – most of this will probably be moved up to that point and referenced at a later stage...]

The raw format for the TPC data is complicated and has many levels of structure. Refer to Figure 6.4 during the following description. The 2048 channels are readout out by 16 front-end boards (containing the cold electronics, including the digitisers), each processed by an RCE and then read into the DAQ by a board reader. The format at this point is referred to as a millislice; there is a millislice for each of the detector components (RCEs, SSPs and PTB) and an ‘event’ is a collection of all such millislices. For the TPC data, a millislice contains all the information for 128 channels. This data also has further substructure; a millislice is composed of N microslices, with each microslice containing M nanoslices. A nanoslice contains 128 ADC values, representing one ‘tick’ (500 ns) worth of data for 1/16th of the detector. A microslice thus contains this information for a ‘drift window’ (M ticks) and a millislice a collection (M) of drift windows. For the normal data running, N was set to 20 and M 1000.

As the detector collects data, the RCEs continually create and save microslices to send to the DAQ to form a millislice. These microslices are empty (contain no nanoslices) until a trigger is received, at which point nanoslices are made and saved within each microslice. There is also a buffer in place to save a certain number of full microslices (microslices containing nanoslices) before the microslice containing the trigger. A certain number of full microslices proceeding the trigger are also recorded by the RCEs. During normal running, a ‘4 + 1 + 10’ format was employed; four microslices containing nanoslices before the trigger was received, the microslice containing the trigger, and the ten following microslices. It should be further noted that, since the DAQ was designed for continuous data readout, these microslices need not necessarily be within the same millislice: it is possible for the trigger to occur in microslice 18 of a certain millislice, resulting in the 15 filled microslices straddling successive millislices. This is demonstrated in Figure 6.5.

Note this also results in real ‘physics events’ being saved in separate ‘DAQ events’; for this reason a splitter/stitcher module has been designed to extract the actual triggered events from the raw data and repackage them into a useful event structure – this is the first stage before all offline analysis with the 35 ton data.

Since the event display runs online, a suitable selection must be applied to ensure the full physics event occurs within the current DAQ event; proceeding and preceding events are inaccessible to the DAQ during running. This is achieved by noting whether or not a trigger occurred (i.e. microslices contain nanoslices) when reformatting the RCE data in DataReformatter, and which microslice it occurred in. For the event display, a triggered event

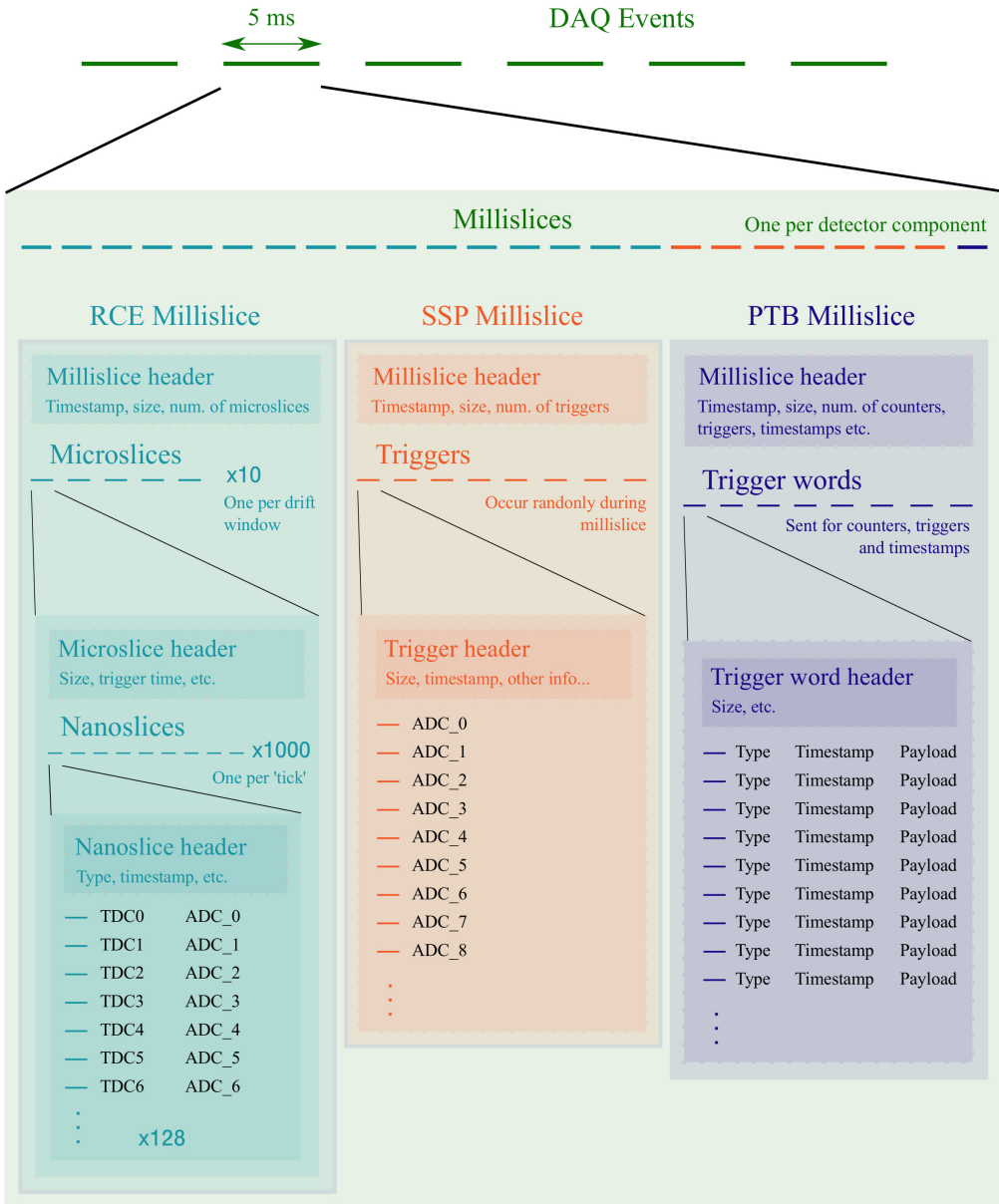


Fig. 6.4 Demonstration of the format used in 35 ton raw data. A ‘DAQ event’ is composed of a single millislice from each component, each containing further substructure unique to the readout elements.

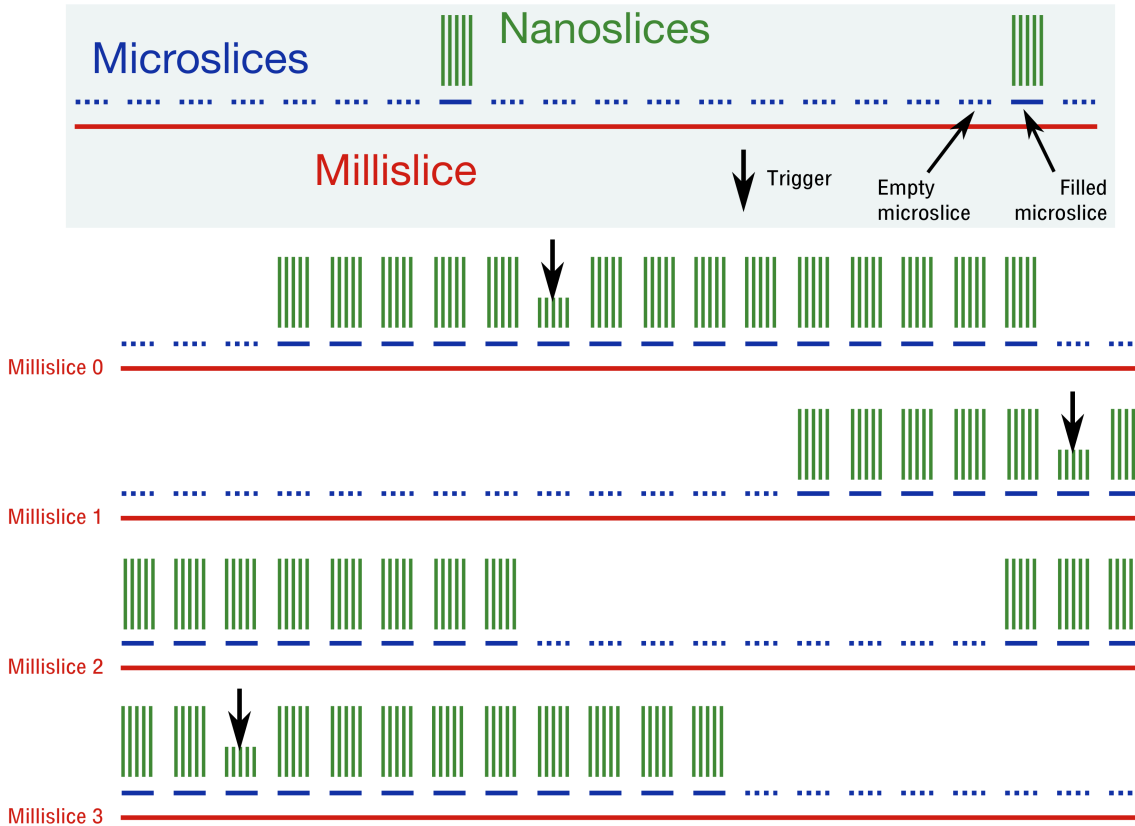


Fig. 6.5 Demonstration of how TPC data is saved when using a DAQ designed for continuous readout. The black arrows represent hypothetical triggers occurring within the duration of a particular millislice. In each case, the 4 preceding microslices and the 10 proceeding microslices are filled with nanoslices and saved; all other microslices are saved with no nanoslices since they contain no useful data. An example of such an event is shown occurring in millislice 0 in the figure. As described in the text, a trigger can cause the useful microslices to straddle consecutive millislices; this is represented in the following millislices in the figure.

is only useful if the trigger occurred within a certain range (e.g. microslice 5 to microslice 10); this ensures all the filled microslices are present within the current millislice. The event displayed is then filled for a given range of microslices around the trigger to capture all the actual physics data.

### 6.4.2 Representing the Data

[This section requires background of reconstruction – this will be the previous chapter.]

Due to the wrapped nature of the induction wires in the 35 ton, and disambiguation being impossible without full reconstruction, it makes little sense to look at charge deposited on

these planes. This results in only the collection planes being useful for showing the data in this way, meaning just one dimension. A second dimension is possible if the view is changed to show a representation of the TPC from above and using the drift time as a coordinate. This requires the two centre APAs be shown together as one combined readout structure. A ‘global collection wire’ is defined by numbering the wires across the APAs, leaving a space for the gaps in between, and used to represent the dimension across the TPC. The drift time, in ticks, represents the second spacial coordinate once charge collected in the short drift volume has been corrected to a negative tick.

By working with the system used to record pedestal values of the channels, it is possible to perform an approximate pedestal subtraction on the data. Whenever a pedestal run is performed by a shifter, a text file containing all the calculated pedestal values for each channel is created and subsequently uploaded to a database for offline use. By making sure a copy of the most recent pedestal file is always available to the monitoring framework, it is possible to always represent the charge as accurately as possible. It is then ensured the pedestal-subtracted ADC values are within the range 0 – 250 to limit the noisy channels and correct for any accidental negative charge. Finally, given the relatively low signal-to-noise ratio, it was decided a grey-scale image showed the best resolution for seeing tracks traverse the cryostat.

An example event display is shown in Figure 6.6.

## 6.5 Monitoring Web Interface

The output of the monitoring is vital in assuring the experiment continues to take high quality, analysable data. To facilitate the monitoring, a web interface was developed to enable all useful information to be displayed on the web and allow convenient, universal access. This interface, along with the complementary web page, was relatively basic but certainly functional and delivered all expected of it for the purposes of a short prototype run. The method of automating the transfer of the monitoring data from where it was saved by the DAQ process to somewhere accessible by the web server is briefly described in Section 6.5.1 and the web page itself discussion in Section 6.5.2.

### 6.5.1 Automated Data Transfer

The most complicated part of the web interface was ensuring the monitoring output were available in the correct place when needed. This is achieved using a combination of disk mounting and automated scripts, demonstrated in Figure 6.7.

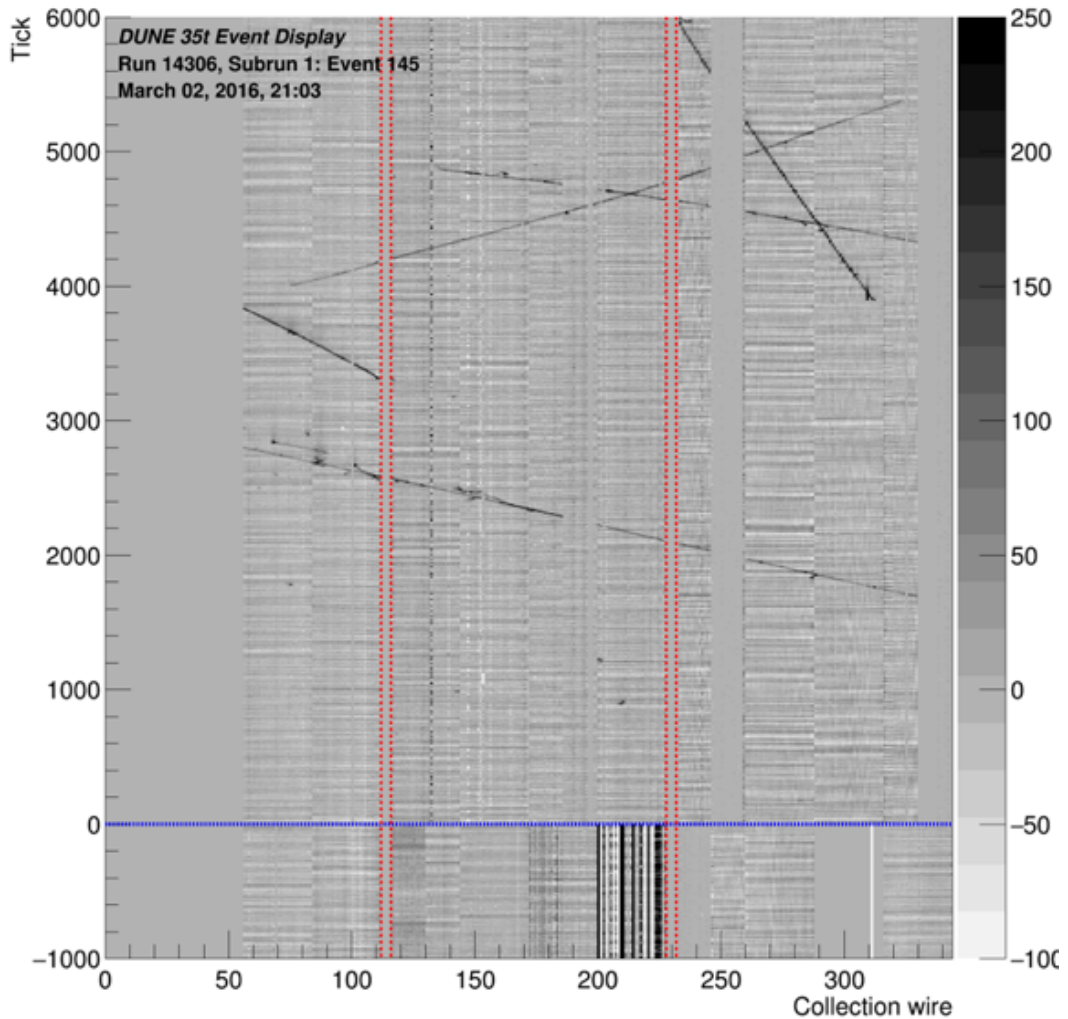


Fig. 6.6 Example online event display made as part of the online monitoring framework for run 14306 (2nd March, 2016). The view is from the top of the detector looking down; the red lines represent the spaces between the APAs and the blue line the location of the APA frames, separating the long and short drift regions.

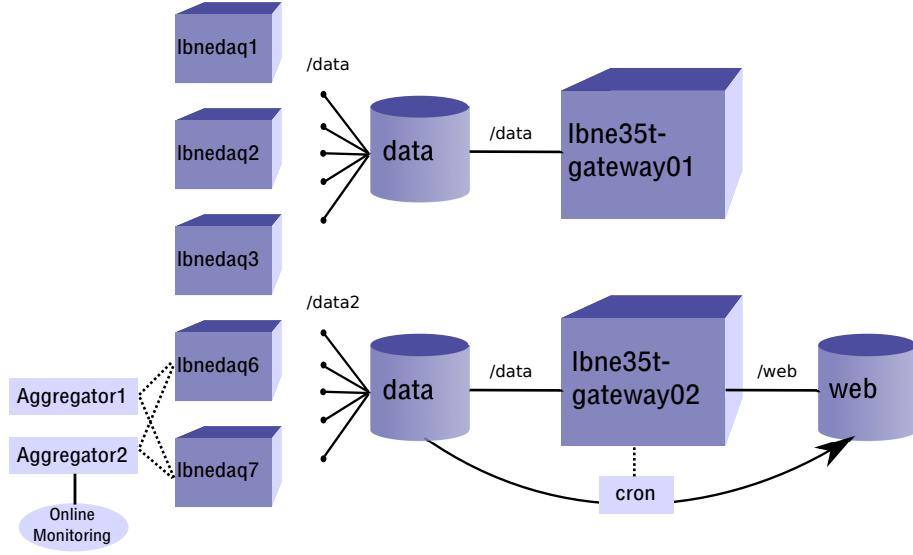


Fig. 6.7 Schematic showing the interface between the online monitoring system and the web. The DAQ machines are shown as rectangles with their disks represented as cylinders. Connections between a node and a disk are shown as straight lines, with dotted lines representing processes running on the machine.

The DAQ aggregator processes run on the lbnedaq6 and lbnedaq7 nodes, requiring any saved output be put in a place which is accessible to these machines. The solution which was developed was to mount a data disk belonging to lbne35t-gateway02 onto these private nodes and save all relevant information there. The constraints placed on the configuration by the DAQ group, which preferred nothing other than DAQ processes to run on lbne35t-gateway01, required a second gateway node to be utilised to move the files off the private network. Using lbne35t-gateway02 also allowed the Fermilab web area to be mounted, with an automated job utilised to copy the monitoring output from the data disk to the specific area on the web server. The frequency of this job, 30s, defined the maximum latency one could expect between data being written out and images appearing online.

### 6.5.2 Web Page

The web page was hosted at FNAL and located at [lbne-dqm.fnal.gov](http://lbne-dqm.fnal.gov). The method in the monitoring framework used to write out all the output also wrote and saved all the HTML used to allow images of the plots to be displayed on the web. This HTML is copied, along with all the images and data files, to the web area as discussed above in Section 6.5.1. The web page was basic but performed all required for use in the 35 ton; it had dedicated pages for all the data quality monitoring information and the online event display (the nearline

monitoring was also hosted at this website but is not described here). See Figure 6.8 for a demonstration of web page and example navigation.

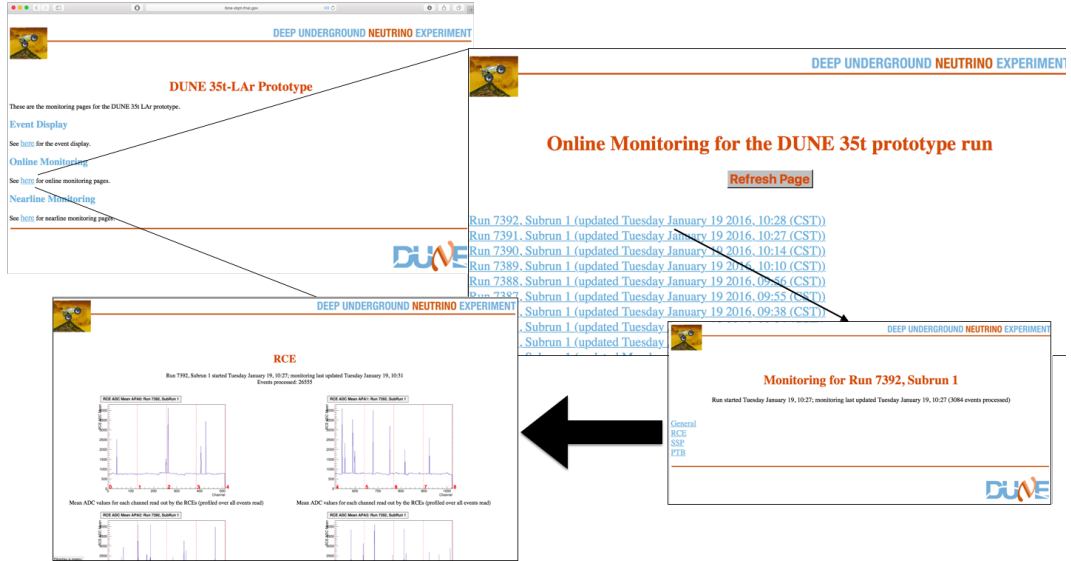


Fig. 6.8 Demonstration of the web page developed to display information produced by the online monitoring and event display. The pages are written in HTML and allowed prompt and convenient feedback directly from the DAQ be accessed anywhere and assist in remote monitoring of the experiment. All previous runs are also kept on the website for reference.

## 6.6 Online Monitoring Summary

The monitoring, with web support, was imperative for the success of the 35 ton. During the ongoing vertical slice tests during summer 2015, the majority of the setup was in place and enabled progress in testing and signing off the APAs to be completed months faster than it otherwise would have been. During this time, and also during commissioning, this framework was the only way of analysing the data without reading it into LArSoft and writing specific software. Overall, the framework provided essential feedback and contributed positively towards DAQ uptime during the data taking period. It is currently in the process of being adapted for future use in DUNE, specifically as part of the ProtoDUNE DAQ for the run in 2018.



# **Chapter 7**

## **Analysis of 35 ton Data**

The 35 ton run (see Section 4) provided 22 days of good quality (high purity, stable field (250 V/cm), stable DAQ), analysable data. Due to the issues encountered, high quality physics analyses proved very challenging and instead more time was taken developing software to mitigate issues such as coherent noise and digitiser stuck bits. Analyses, particularly those presented here, focused on trying to understand the detector and characterise previously untested responses. In this respect, the 35 ton proves to be a vital experiment in informing the next generation of prototypes and even the final DUNE far detector design. It also boasts datasets which no planned experiment will have before the full DUNE modules; it is therefore essential as much information as possible is extracted from the 35 ton analyses.

Before analyses are presented, techniques developed to enhance the quality of the data, and the data selection, will be discussed in Section 7.1. A short section demonstrating how LAr purity may be determined from data is contained in Section 7.2 before the main analyses, concerning tracks passing through the APA frames and across APA gaps, are presented in Section 7.3 and Section 7.4 respectively. Finally, a brief investigation into the performance of basic shower and calorimetric reconstruction on the 35 ton data is discussed in Section 7.5.

### **7.1 Preparing 35 ton Data for Analysis**

To ensure analyses are as accurate as possible, careful pre-selection and preprocessing of the data is performed. Methods for producing the analysable sample are discussed in the section.

### 7.1.1 Selecting the Data

The level of noise present in the TPC data varied hugely between runs – this is evident from analysing the RMS of the charge read out on a particular channel. Figure 7.1 shows a comparison of this metric for ‘good’ and ‘bad’ runs.

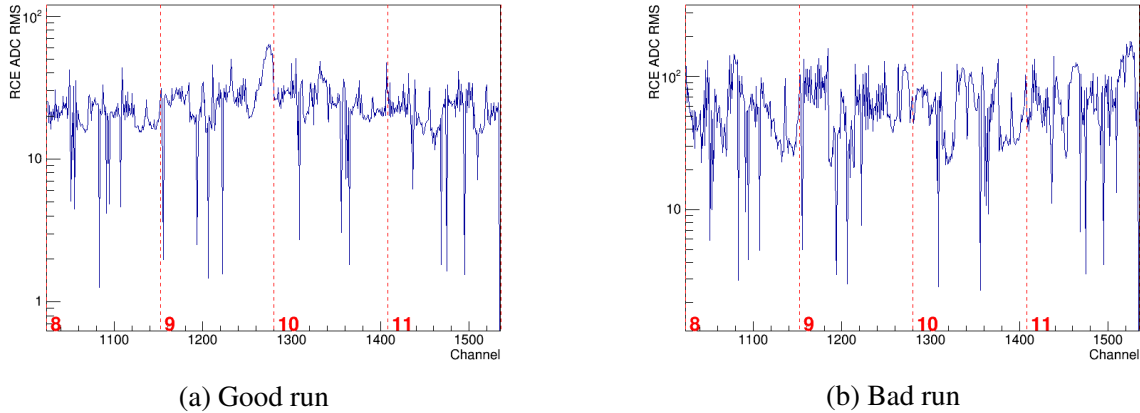


Fig. 7.1 Comparison between noise levels for ‘good’ and ‘bad’ 35 ton runs. The channels shown are on APA2 (online convention, APA0 offline) and are read out by RCEs 8 through 11 (labelled). The increase in read out charge RMS is evident in the case of the noisy run. These plots are from runs 15797 (Fig 7.1a) and 15790 (Figure 7.1b) and were taken only 50 minutes apart.

Runs which exhibited the lowest noise were selected for analysis. In all there were 1269 runs used representing some data taken before the FNAL site wide power outage (3rd March 2016) with most the week after stabilising the experiment again (9th March – 17th March). A selection of bad channels, classified as either ‘dead’ (electrically) or ‘bad’ (exhibit sufficiently more than average noise), represent 8% of the total number of channels.

Due to the continuous nature of data taking, there is a non-trivial correlation between a ‘DAQ event’, a collection of fragments read out by the DAQ, and a ‘physics event’, an event in which particle interactions occurred. The external triggers used in the 35 ton, namely the external muon scintillators and the photon detectors, are used to define the event time. Given the trigger rate at which most data was taken ( $\sim 1$  Hz), a typical run comprising a few thousand events will only contain  $\mathcal{O}(10)$  triggered events. Furthermore, given the data format, these events often straddle multiple DAQ events (refer to Figure 6.5 for a demonstration of this). A splitter/stitcher module is employed to search for triggers within runs and construct physics events containing the useful information for analysis. This produces a file with just this relevant information, which are then used for analysis.

### 7.1.2 Improving Data Quality

Two issues present in the raw data, namely the presence of correlated noise and the stuck bits in the digitiser, are dealt with as an initial step of the reconstruction. First, an algorithm attempting to correct for the stuck bits analyses waveforms on a wire and identifies problematic ADCs; interpolating between charges read out at neighbouring times is successful at reconstructing the initial waveform in most cases. Figure 7.2 demonstrates this interpolation method on simulated data.

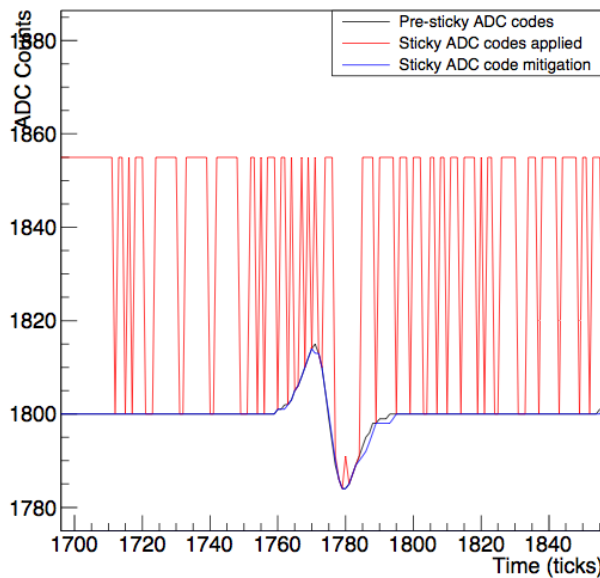


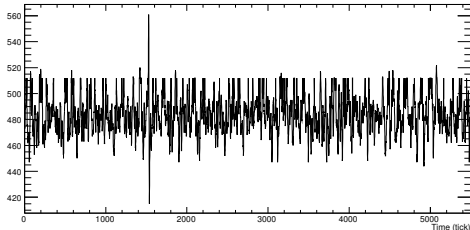
Fig. 7.2 Simulated demonstration of the method used to correct for stuck codes in the 35 ton data. On a given channel, ADCs exhibiting the consequences of this problem are corrected by interpolating charge at neighbouring time units. This is tested by simulating a waveform and adding the observed stuck code effect; the efficacy of the method at correcting the afflicted bits can then be evaluated.

The effect of applying this algorithm on a full waveform, to correct for all the stuck bits, is apparent in Figure 7.3.

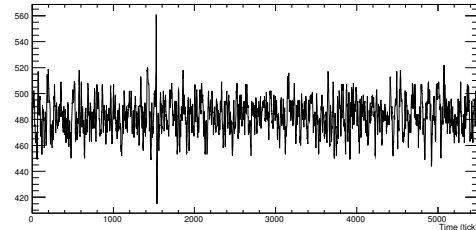
Following this process, a coherent noise removal stage is applied. This simply looks at the average noise across channels sharing a front-end voltage regulator and removes this component from the readout ADC for each channel. The effect of this correction is seen in Figure 7.4.

### 7.1.3 Reconstructing Muon Tracks

All analyses discussed below only make use of information recorded on the collection planes. Since the induction wires are longer (a necessity for wrapping), a larger capacitance

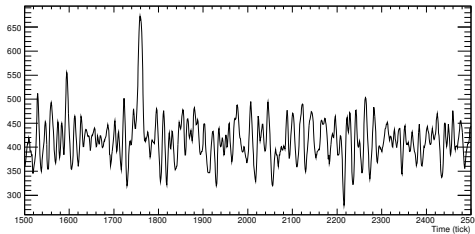


(a) Raw waveform before correcting for stuck bits.

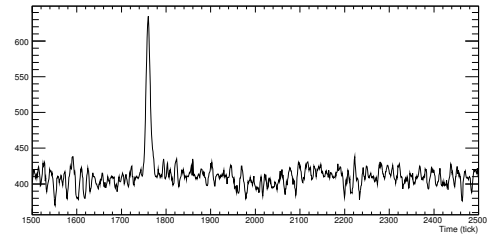


(b) After applying stuck bit mitigation.

Fig. 7.3 The effect of applying stuck bit mitigation to a waveform as seen in raw data. This particular waveform is from run 15660, channel 722 (induction channel).



(a) Waveform before removing coherent noise.



(b) After removing coherent noise.

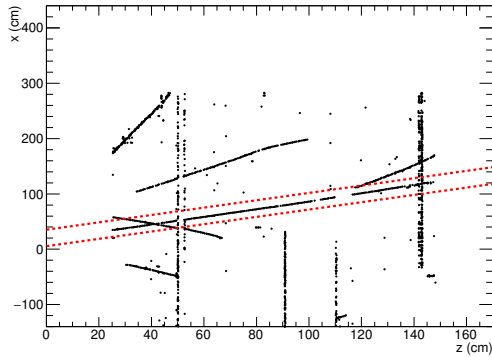
Fig. 7.4 The effect of removing coherent noise from all channels on a voltage regulator. This waveform is from run 15660, channel 2010 (collection channel). The signal is noticeably larger following this process, considerably improving reconstruction performance.

results in higher noise levels, complicating the reconstruction. In general, after applying the refinements outlined in Section 7.1.2, the signals on the collection channels are prominent enough for competent analyses. The methods used to select tracks are described in this section and applied during the subsequent studies.

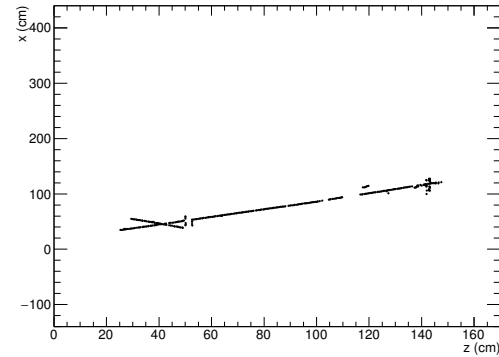
Using only the collection plane presents challenges, the most obvious being the impossibility of full 3D reconstruction. A hit on a collection wire at a given time gives well-defined  $x$  and  $z$  coordinates but cannot give any information in the  $y$ -direction. ‘Quasi-3D’ reconstruction is achieved by making use of the external counters. Through-going muons are triggered by the coincidence of hits in two opposite counters; this information can be used to give a crude handle on the  $y$  position of hits.

Figure 7.5 outlines the stages of selecting hits originating from the particle track which caused the trigger. Figure 7.5a shows all hits from an example event containing a through-going muon. The first stage of track selection involves taking those hits which lie in the ‘counter shadow’, the narrow section of collection plane area physically inbetween the opposing counters through which the triggering particle passed. The hits which remain are

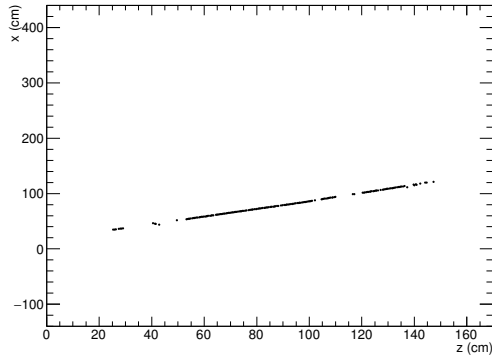
shown in Figure 7.5b. The track hits are visible along with further, unrelated hits. These are removed by requiring that only hits on wires with single occupancy be kept, and then applying a linear fit and removing all hits with residual  $> 2$  cm. The final output after these stages is shown in Figure 7.5c.



(a) All hits before any track selection. The red lines represent the boundary defined by the edges of the two counters causing the trigger.



(b) Hits in the counter shadow.



(c) Hits on single wire occupancy and with residual  $< 2$  cm.

Fig. 7.5 Demonstration of the successive stages applied to hits on collection wires in order to select hits from the through-going track associated with the particle which caused the trigger. The hits left after all stages are taken forward into the analyses.

The result of this track selection, as evident from Figure 7.5c, is a well-formed, high quality track with which it is possible to perform analyses. These will be the focus of the remainder of this chapter.

## 7.2 Measuring LAr Purity from Crossing Muons

### 7.3 APA-Crossing Muons

The 35 ton is the only proposed experiment before the full DUNE far detector modules that have fully implemented anode planes within the cryostat reading out data from multiple drift regions simultaneously (ProtoDUNE will have wrapped wire APAs but will only read out one drift region each and SBND has the CPAs in the centre of the cryostat with the APAs at the edges). Referring to Figure ??, this is a design consideration that features prominently in the eventual detector so any implications in the data must be well understood. Analysis of tracks which pass through the APAs and deposit charge in both drift regions is the subject of this section.

In Section 7.3.1, a method to determine the absolute event time, T0, from APA crossing tracks is presented and in Section 7.3.2 the charge deposited by these tracks, particularly when crossing through the planes, is studied. Comparisons between the two drift regions, made possible by comparing tracks left by the same particle, are contained in Section 7.3.3.

#### 7.3.1 T0 Determination from APA Crossing Tracks

Given the nature of a TPC detector, an ‘event time’ (T0) must be known in order to set an absolute timescale, and therefore absolute position, on all interactions within the detector. An accurate T0 is essential for calorimetric reconstruction: in order to understand how much charge a hit had when it was created, a lifetime correction dependent on the total drift time must be applied. An incorrect T0 would lead to a systematic under- or over-estimation of the reconstructed energy and have implications in particle identification and shower energy determination.

In a LArTPC, an event time is usually given by an external triggering system. The DUNE far detector will rely on the instantaneous detection of photons produced from the immediate recombination of the ionisation electrons with positive Ar ions. In the 35 ton, an additional external system was provided by the scintillation counters. Since the sample of APA crossing muons used in this analysis were all selected and reconstructed using counter information, an interaction time is immediately known.

Without correctly accounting for T0, the tracks on each side of the APAs appear offset from the planes. This is evident from the event display shown in Figure 7.6. By aligning the track segments on either side of the APAs, a measurement of T0 can be made directly from the TPC data.

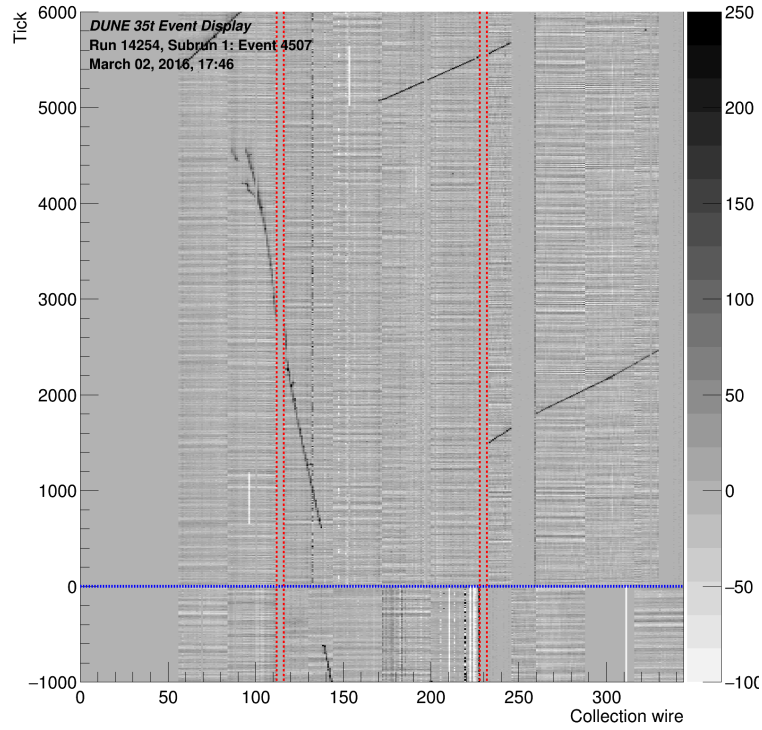
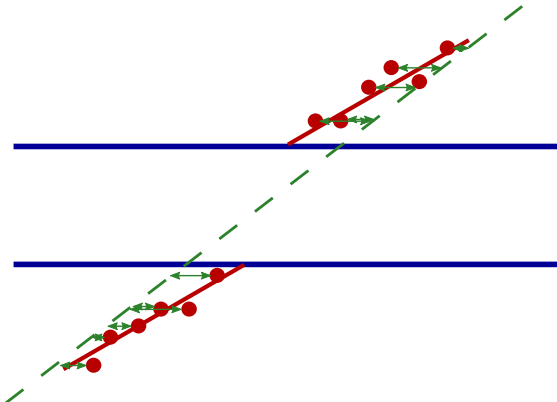


Fig. 7.6 Event display made during the run in which a track passes through the APAs. Correcting for  $T_0$  would eliminate the visible offset and result in a single accurately connected track.

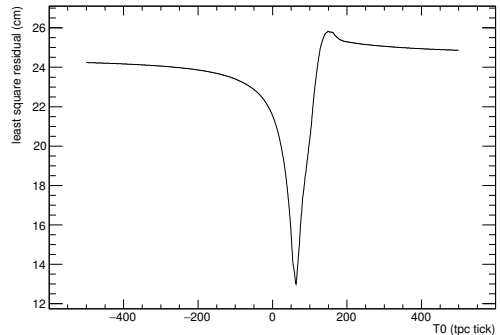
### 7.3.1.1 Aligning APA Crossing Tracks

Two complementary methods were used to accurately align the track segments across the APA. Both involved initially correcting for the counter  $T_0$ ,  $T_0^{\text{counter}}$ , before considering a range of alternative  $T_0$  hypotheses and minimising a relevant metric to determine the most likely value. In the first method, demonstrated in Figure 7.7, a least square linear fit is applied to the track and the residual minimised. The second method, demonstrated in Figure 7.8, involves fitting a line to each segment in turn and minimising the projected distance between the intersections of the lines with the centre of the APAs ( $x = 0$ ). As will be shown later, and can be seen from Figs. 7.7b and 7.8b, the two methods agree very well with each other.

Naively, one would expect the  $T_0$  determined using these methods,  $T_0^{\text{TPC}}$ , to agree with  $T_0^{\text{counter}}$ . It was noted however that there appeared to be a systematic offset between the  $T_0$  given by the counters and measured from the TPC data. The distribution of this disparity is shown in Figure 7.9; it peaks very sharply around 64 ticks (32  $\mu\text{s}$ ) and is importantly inconsistent with zero. This suggests an inconsistency somewhere in the data taking and will be the subject of the remainder of this section. Figure 7.10 shows an example track before and after this disparity is corrected for.

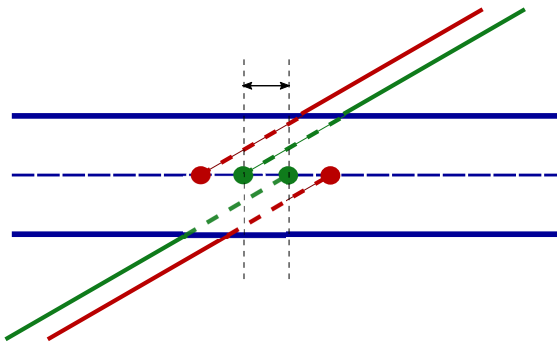


(a) Demonstration of the calculation of residuals from a linear fit through all hits. The red points are hits and the green line represents a linear fit through all points on both sides of the APA.

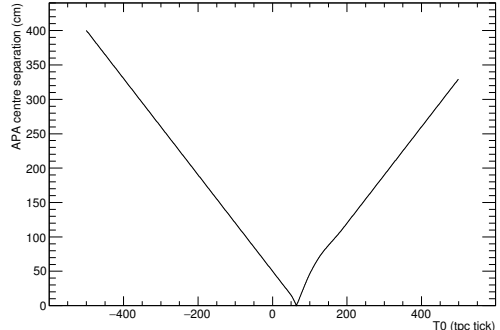


(b) The residuals to the linear fit of the track over a range of  $T_0$  candidates. The value of  $T_0$  which minimises this distribution (62 ticks in this case) is considered the most likely interaction time.

Fig. 7.7 Method to align track segments on either side of the APAs involving minimising residuals from a linear least square fit. A fit is applied to all hits and the resulting residual, a representation of the ‘goodness of fit’, is minimised over a range of  $T_0$  candidates to find the most likely interaction time for the particle leaving the track.



(a) Demonstration of the determination of the distance between the track segments at the centre of the APAs. The red and green lines represent linear fits to the hits (applied separately on each side of the APA) for different values of  $T_0$ .



(b) The separation distance over a range of  $T_0$  candidates. The value of  $T_0$  which minimises this distribution (63 ticks in this case) is considered the most likely interaction time.

Fig. 7.8 Method to align track segments on either side of the APAs involving minimising the distance between the projected intersection of each with the centre of the APAs. A fit is applied to each track segment separately and the distance between the intersection of these lines with the centre of the APA is minimised over a range of  $T_0$  candidates to find the most likely interaction time for the particle leaving the track.

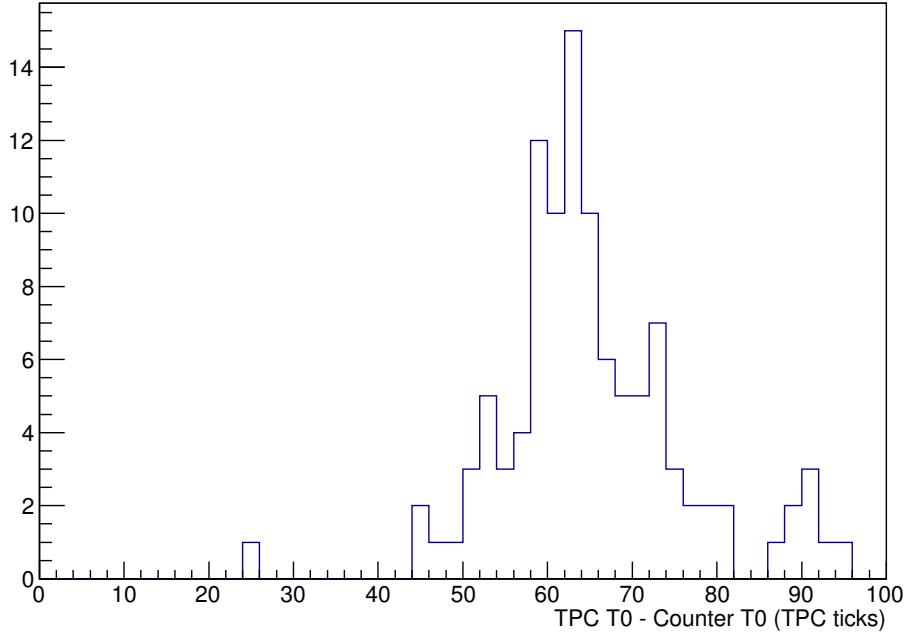


Fig. 7.9 [Placeholder image until I get one with full stats again!] Difference between the  $T_0$  calculated from TPC data and the  $T_0$  provided by the counters representing the trigger time of the through-going muon. If the two measurements of  $T_0$  agreed the distribution would peak at zero; the fact it does not is indicative of a systematic offset somewhere in the data taking.

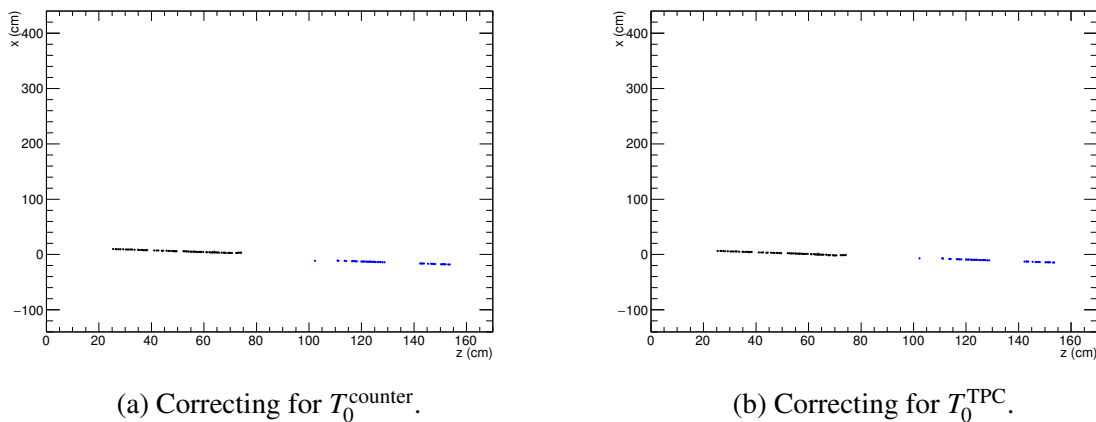


Fig. 7.10 Correcting for  $T_0$  using  $T_0^{\text{counter}}$  (Figure 7.10a) and  $T_0^{\text{TPC}}$  (Figure 7.10b). The difference is subtle but obvious; the method for determining  $T_0$  directly from the TPC data can be validated by eye. The minimisation of the metrics to determine  $T_0^{\text{TPC}}$  in this case are demonstrated in Figs. 7.7b and 7.8b.

Attempts to understand the misalignment of the tracks across the APAs are presented in the remainder of this section.

### 7.3.1.2 Understanding the Misalignment of APA Crossing Tracks

The underlying issue described above is essentially a misalignment of the same particle track between the two drift regions (see Figure 7.11). This obviously is not physical and stems from an issue with the detector or data readout. The most obvious cause is a miscalibration of the DAQ timing systems for the separate detector components, as previously assumed; there are however other possible causes for this problem. Most likely, the effect arises from a combination of these different factors.

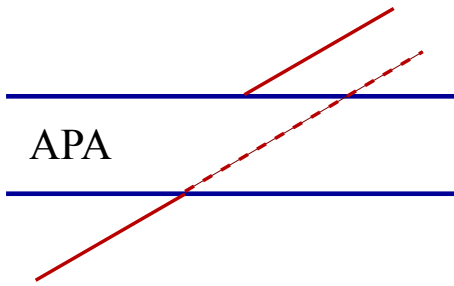
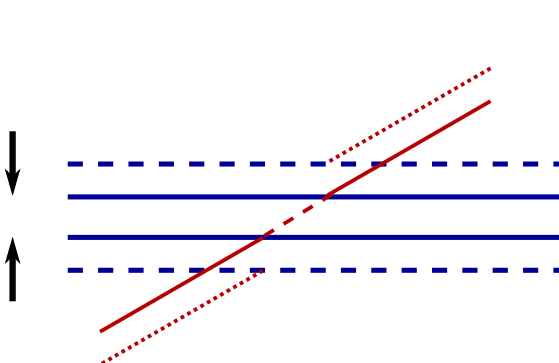


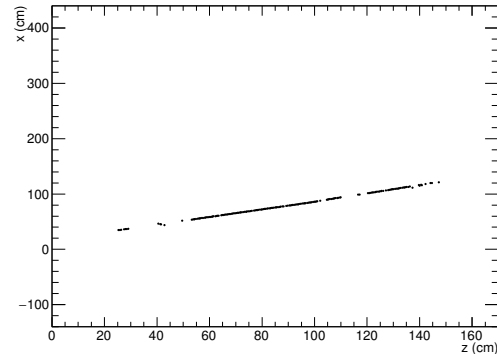
Fig. 7.11 (Possibly unnecessary, but helps to explain all the various factors which could explain the offset. Can remake if necessary.) Demonstration of the effect observed in the 35 ton data concerning tracks crossing the APAs. Even after correcting for the T0 provided by the counters, there is still a misalignment of the track segments across the APA frames.

**Geometry** Apart from timing, a misunderstanding of the geometry could explain this perceived misalignment. The spacing between the collection planes is one such example, as demonstrated in Figure 7.12a; the spacing necessary to explain this effect, determined by aligning the tracks using the methods discussed above over a range of collection plane spacing hypotheses, is demonstrated in Figure 7.12b. As is evident from the figure, the collection planes must be repositioned in such a way that they would be reversed; the track alignment complications cannot be explained solely by this.

A further problem is related to the wire positioning on the APAs in the  $z$ -direction; it is understood there may be a discrepancy between the two sides of the APA resulting in hits from the long and short drift regions at the same  $z$ -position reconstructed with a systematic offset. Figure 7.13a shows how this could be utilised to explain the apparent track misalignment with Figure 7.13b showing the distribution of corrected  $z$  positions necessary to resolve the issue. Offsets of  $\sim 30$  cm, as suggested by these results, are impossible, indicating again the track alignment problem cannot be resolved in this way.

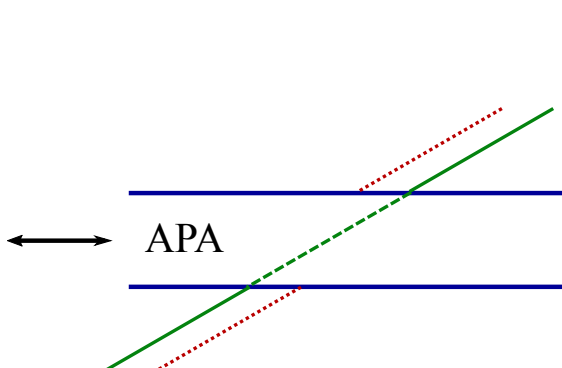


(a) Demonstration of how the track misalignment could be explained by an incorrect collection plane spacing.

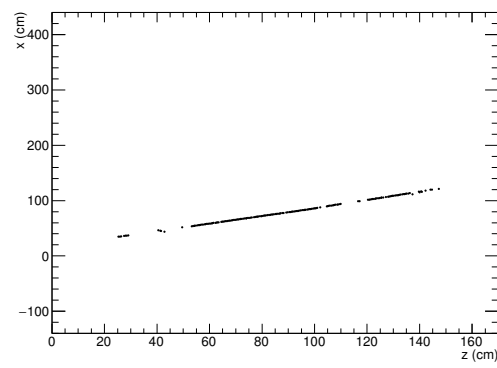


(b) Corrected spacing between the collection planes after considering a range of values and aligning the track segments. The red line shows the spacing used in the geometry.

Fig. 7.12 Attempting to correct the track segment misalignment by assuming a misunderstanding of the spacing between the collection planes. It appears the resulting spacing necessary to correct for this issue would involve physically reversing the order of the planes.

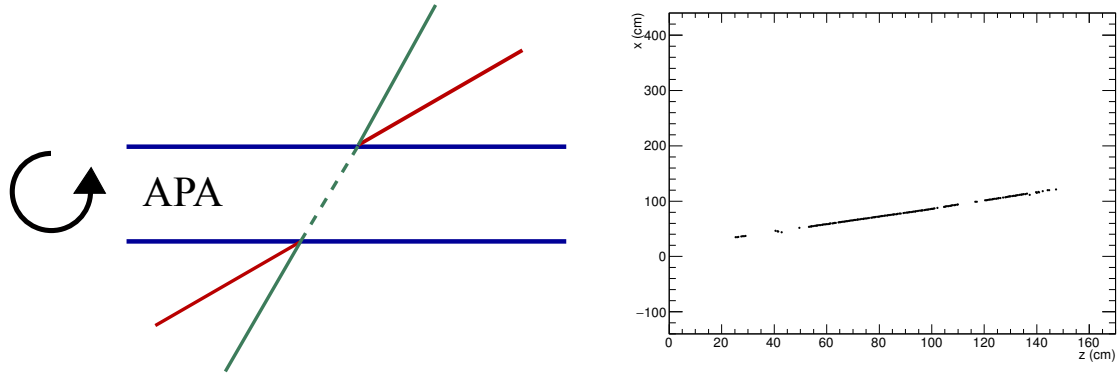


(a) Demonstration of how the track misalignment could be explained by an offset in the wire  $z$ -position on either side of the APA.



(b) Corrected  $z$ -positions of the APA wires after considering a range of values and aligning the track segments.

Fig. 7.13 Attempting to correct the track segment misalignment by assuming a misunderstanding of the positioning of the collection wires inside the detector. The wire offset would have to be around a foot to fix this issue.



(a) Demonstration of how the track misalignment could be explained by an incorrect drift velocity.

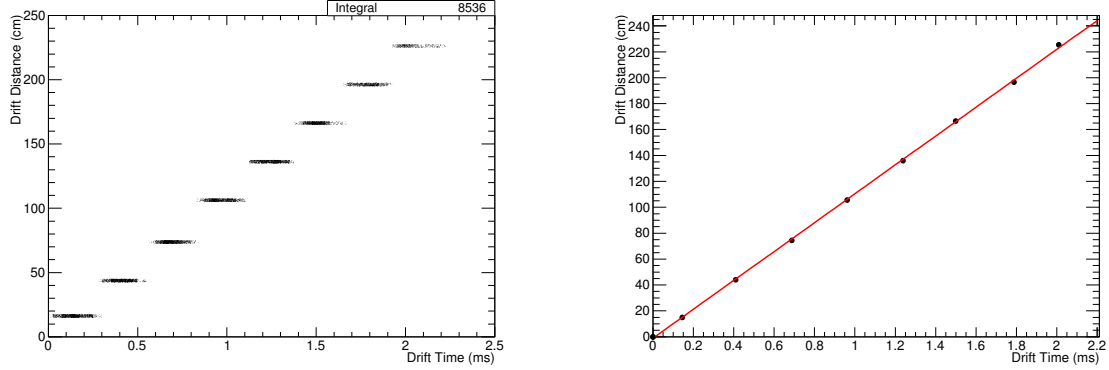
(b) Corrected drift velocity required to align the track across the APAs.

Fig. 7.14 Attempting to correct the track segment misalignment by assuming an incorrect drift velocity. In order to account for the effect noted in the data the drift velocity would have to around five times larger than that initially calculated from models.

**Drift velocity** The drift velocity affects the angle of the tracks in wire/time space; a high velocity would result in a refraction-like effect towards the APA planes. As demonstrated in Figure 7.14a, this could explain the track segment misalignment if the effect was large enough. Figure 7.14b shows the necessary drift velocity required to account for the disparity observed in data; compared to a nominal value of 109 cm/ms, the scale of the change required to explain the oddity is unreasonably large.

This can be tested by measuring the drift velocity directly from the data. Taking tracks which pass through opposite counter pairs and comparing this drift distance with drift time is a trivial exercise, demonstrated in Figure. 7.15. The measured value of 110 cm/ms agrees exceptionally well with the aformentioned value, determined theoretically, of 109 cm/ms. It may therefore be assumed the drift velocity is as expected and does not contribute at all to the track alignment anomoly.

**Timing** The timing offset calculated in Section. 7.3.1.1,  $32 \mu\text{s}$ , is so large it was assumed another explaination for the track segment misalignment was likely. However, after reviewing all possibilities it appears there must be a significant timing offset present somewhere in the data. Further evidence for this hypothesis is presented in Figure 7.16 which displays the T0-corrected time distribution for all hits on the APA crossing track. The minimum drift time these hits may have, since they pass directly through the planes, is the interaction time, T0. As is evident from the distribution in Figure 7.16b, this is around 56 ticks ( $28 \mu\text{s}$ ) and is



(a) Distribution of hit drift times for eight sets of counter pairs, assuming all tracks pass through the centres of the counters.

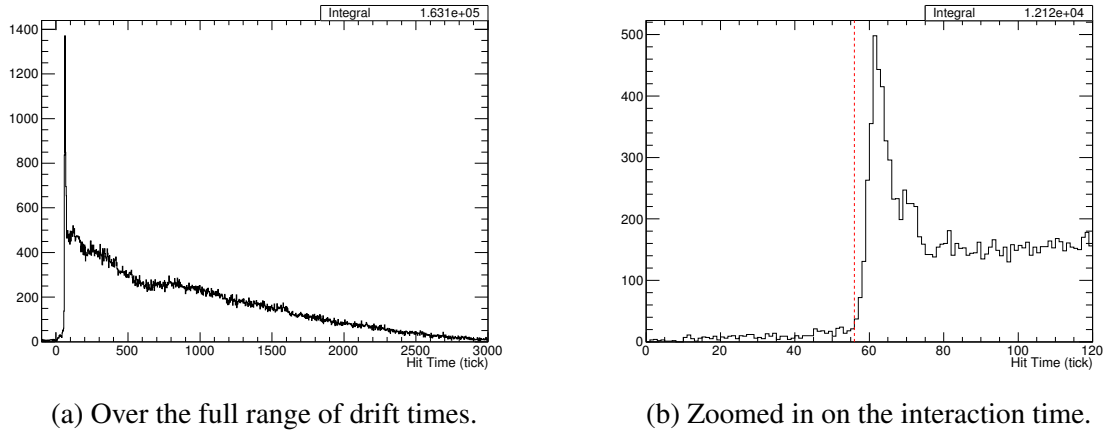
(b) The eight points found from taking the Gaussian mean of the time distributions for each rough drift distance.

Fig. 7.15 Measuring the drift velocity of the ionisation electrons by taking tracks passing through opposite counter pairs and comparing the corresponding drift distance to the drift time. Assuming all tracks pass through the geometric centres of the counters, a poor assumption, a distribution of hit time for this drift distance can be found; this is shown in 7.15a. Taking each counter pair separately and fitting a Gaussian to the distribution of drift times nullifies the assumptions necessary due to a lack of exact knowledge, on a track by track basis, of the exact  $x$ -position. This is shown in the graph in Figure 7.15b.

notably inconsistent with zero. The curious spike at the interaction time motivates the work presented in Section 7.3.2 and will be discussed there.

This interesting result provoked further investigation into the notion of a timing offset between detector components, specifically the TPC and counter readout (RCEs and PTB respectively). Confirmation of this miscalibration is displayed in Figure 7.17 which shows the difference between the timestamps recorded by each of the subcomponents upon receiving the trigger.

Within the limitations of all methods discussed, there is agreement between the T0 offset in Figure 7.16b and the timing miscalibration in Figure 7.17. This does not however account for the full track segment misalignment; this represents 64 ticks ( $32 \mu\text{s}$ ) if accounted for using timing alone, as seen in Figure 7.9. As previously noted, the complete solution is likely a combination of different effects. Given that drift velocity and  $z$ -position of wires effects are negligible, the remaining offset must be due to a slight discrepancy between the actual spacing of the collection planes and what is being assumed. With an actual T0 of 56 ticks, this collection plane spacing can be determined in the usual way by aligning tracks. The results of this are demonstrated in Figure 7.18.



(a) Over the full range of drift times.

(b) Zoomed in on the interaction time.

Fig. 7.16 The T0-corrected drift time for hits on APA crossing tracks. The lower leading edge of this distribution is an indication of the interaction time, T0. The red line on Figure 7.16b is drawn at 56 ticks (28  $\mu$ s) and represents, by eye, the start of the distribution.

The misalignment of the tracks, as described in Section 7.3.1.1, can be understood as a combination of a timing miscalibration between two detector components and a slight offset in the geometry, which is not unexpected. This is the first time tracks crossing the readout planes have been used in a LArTPC experiment and have proven to be a valuable way of calibrating inter-detector components and finding other inconsistencies in the data. Without studying this data set, the timing offset between the TPC and the external counters would not have been discovered and all analyses would naively use the incorrect T0. In the next section, another source of information which can be gleaned from this dataset, this time more about understanding detector responses, will be discussed.

### 7.3.2 Charge Deposited by APA Crossing Tracks

The intriguing distribution of the T0-corrected hit times observed in the data, shown in Figure 7.16a, hints at some aspect of the detector response that needs to be understood. In the DUNE far detector, a large number of events will contain particles which pass through the APA frames so characterising resulting effects is critical. The equivalent plot for simulated data, filtered by those triggered using external counters and processed in the same way, is shown in Figure 7.19. Comparing these distributions, there is a very obvious difference around the interaction time. It appears there is an effect present in the data, not currently being simulated, which manifests in around twice the amount of hits occurring at T0 on the collection planes for APA crossing tracks. This is described in Section 7.3.2.1 and the phenomenon is visible on event displays presented in Section 7.3.2.2.

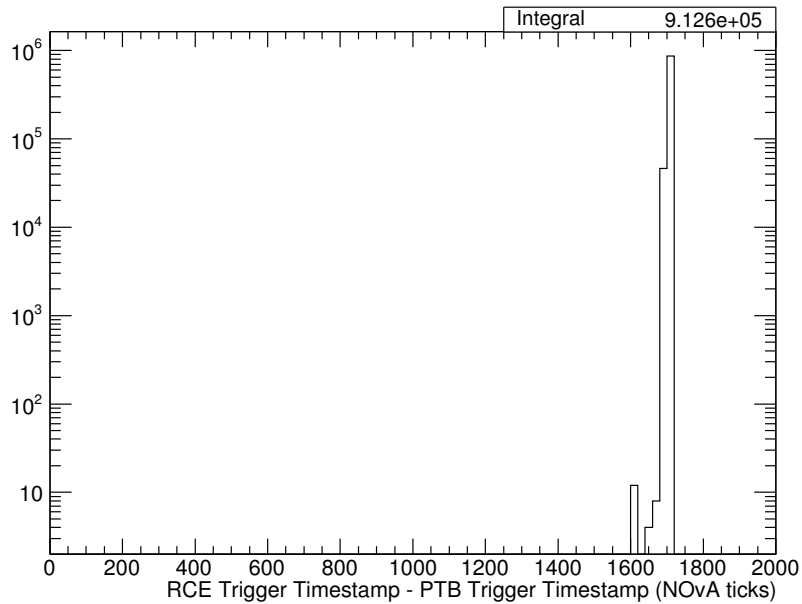


Fig. 7.17 The difference between the timestamps recorded by the PTB and the RCEs upon receiving a trigger. The absolute timing for the DAQ system is given, along with most experiments at FNAL, by ‘NOvA time’: a 64 MHz clock starting on 1st January, 2010 (with one NOvA tick therefore being 15.625 ns). The distribution peaks sharply at 1705 NOvA ticks, or 26.6  $\mu$ s.

Fig. 7.18

### 7.3.2.1 Interaction Time Hits

The excess of hits at the interaction time is due to the use of a grounded ‘mesh’ at the centre of the APAs. The purpose of such a design choice is to ensure a uniform electric field across the face of the APA; without it the field would be ill-defined given the presence of the grounded, rectangular APA frames with positively biased planes on either side. It is plausible therefore to consider a ‘backward-facing’ field being set up between the grounded mesh and the positively biased collection planes which would lead to hits drifting the ‘wrong’ way when produced in this region; APA crossing tracks would hence leave twice as many hits on the collection plane as the other planes. This is demonstrated schematically in Figure 7.20.

A convenient way of confirming whether or not the mesh can explain this excess of hits at the interaction time is possible since one of the four APAs in the 35 ton was constructed without the mesh, precisely for this purpose. Unfortunately, this was the APA which was more plagued by noise issues so very little good data is available from channels on this APAs. It is however possible to make a crude comparison; this is shown in Figure 7.21. The appears

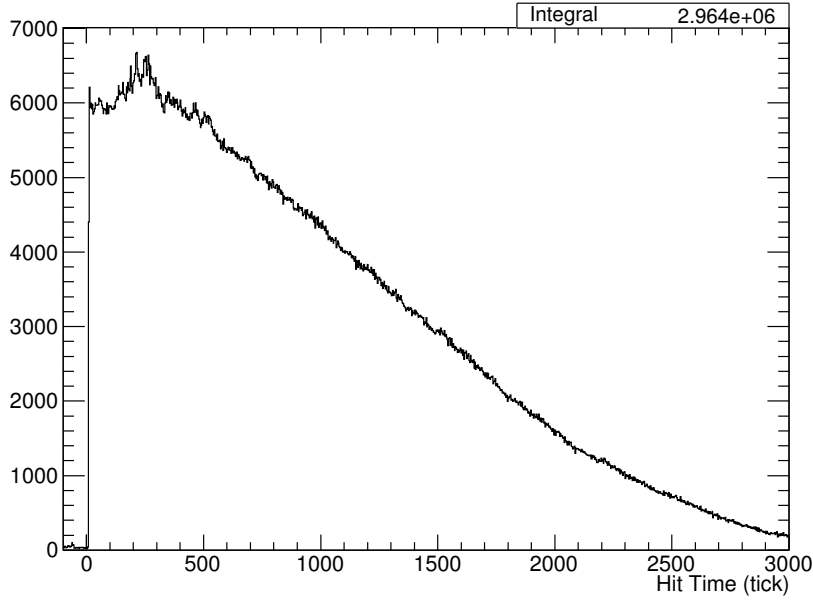


Fig. 7.19 The T0-corrected drift time for all hits on an APA crossing track in simulation. The equivalent plot for 35 ton data is shown in Figure 7.16a.

to confirm the shark peak of hits occurring at the interaction time comes from the APAs which use a mesh.

Using the 35 ton dataset, it is also possible to confirm that the mesh is functioning as expected. Without a mesh, one may expect a difference between the hits deposited on wires towards the centre of an APA face and wires at the edges, in front of the grounded frame. The functionality of the grounded mesh ensures there is no difference between any wires on a given APA. Figure 7.22 confirms this is the case.

A natural question to pose at this point is to ask if these ‘extra’ hits deposited by APA crossing tracks as a result of this ‘backwards’ field have similar properties to the ‘correct’ hits. The most important property to consider is the charge of the hits; Figure 7.23 shows the average charge per hit for hits occurring at the interaction time and all other hits. It is clear from this there is nothing different about these additional hits and they can be treated in the same way.

As alluded to earlier, the DUNE simulation software is simplistic and does not simulate any ionisations within the region of the APA planes; in the case of APA crossing muons this results in no hits being created after the track passes through the first induction wires. Evidently, this is an important region and must be understood and well simulated in order to test reconstruction and analyses. When this is added to the software, the 35 ton data will be essential for validation purposes.

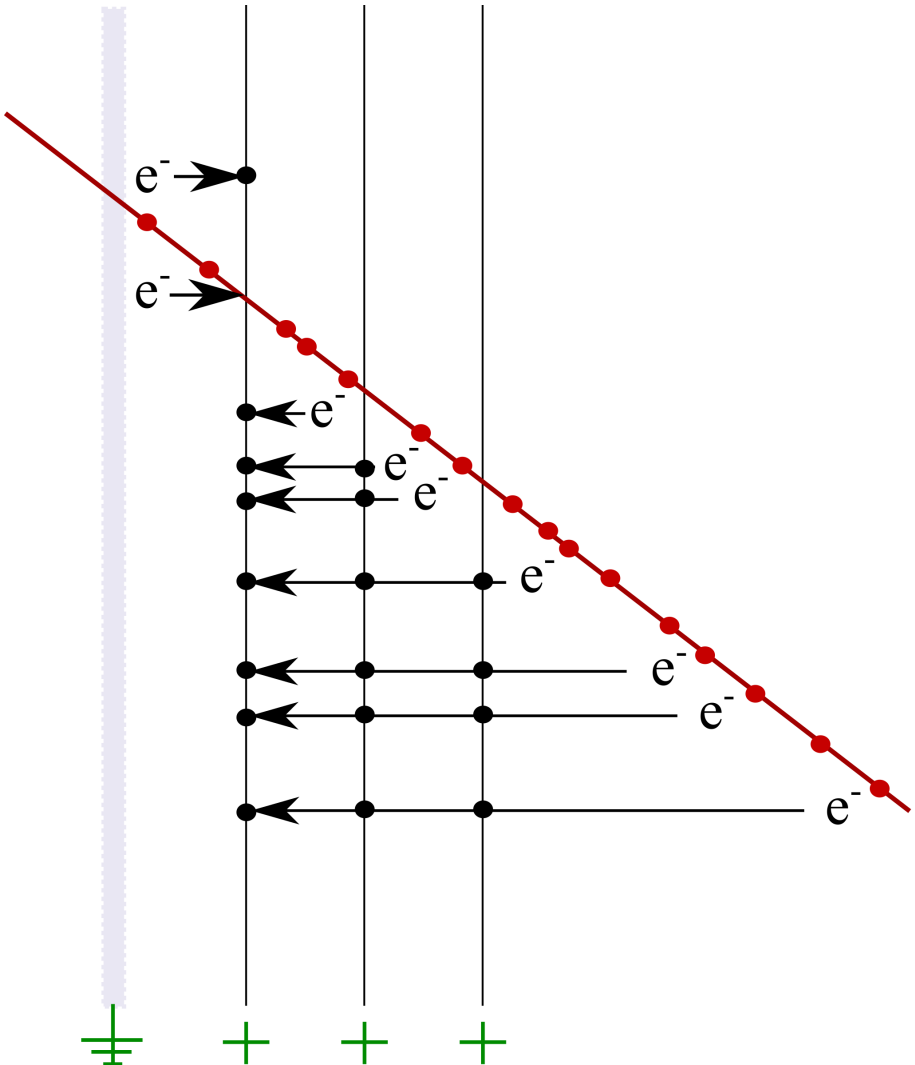
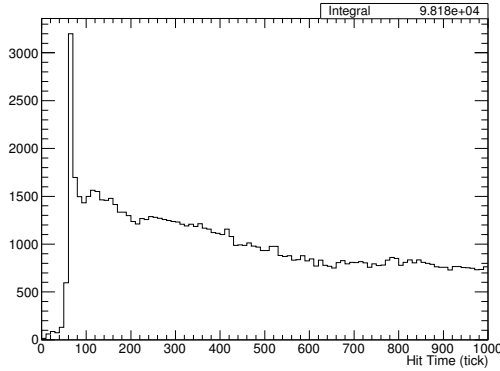
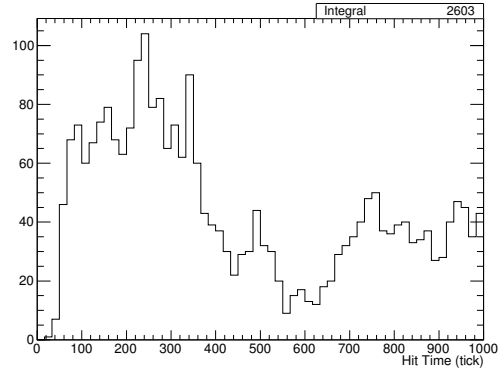


Fig. 7.20 Demonstration of the ionisation and hit collection for APA crossing tracks. The red line represents a track passing through the anode planes, shown in black. The grey region is the centre of the APA frame on which the grounded mesh is afixed. The red dots correspond to the ionisation of electrons which then drift, depositing charge (black dots) on the readout wires. The three planes shown are, from left to right, the collection plane and the two induction planes. The biasing of each of the planes and mesh sets up field lines which all terminate on the collection wires, resulting in charge collected from before the track passes through and after.



(a) Hit times for all hits on APAs 0, 2 and 3; these are the three APAs containing the grounded mesh at the centre.



(b) Hit times for all hits on APA 1, the APA without a grounded mesh at its centre.

Fig. 7.21 Comparison between the T0-corrected hit time distributions on APAs with and without the grounded mesh. Even given the very low stats in Figure 7.21b, there is a noticeable difference in the distribution of hits around the interaction time.

### 7.3.2.2 Event Displays of APA Crossing Tracks

The effect investigated in Section 7.3.2.1 is directly observable in the raw data, as shown in Figure ???. The electrons ionised as the particle track passes between the collection plane and the mesh are observable as hits which appear to have drifted in the negative time direction. The outcome is a little ‘hook’ shape in the data.

### 7.3.3 Comparison Between Drift Regions Using APA Crossing Tracks

APA crossing tracks may be utilised to make unique, specific measurements of the detector made possible since they originate from the same particle. For example, any drift velocity differences between the drift regions may be observed and the noise levels on the collection readouts on either side of the APA can be studied and compared.

The drift velocity is given by the angle of the track in wire/time space and any difference between this velocity in the two drift regions would be noticeable in a refraction-like effect. This is demonstrated in Figure 7.24a. A measure of the angle between the track segments in the different regions would therefore be a measure of the change in drift velocity; this is shown in Figure 7.24b.

The relative noise on the two collection planes can be evaluated by considering the number of hits present in the counter shadow, in each drift region, which were not reconstructed as part of the track associated with the triggering particle. The difference between each

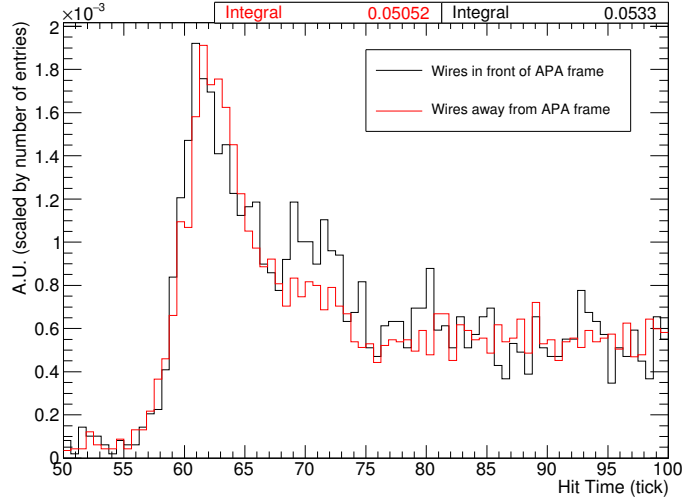
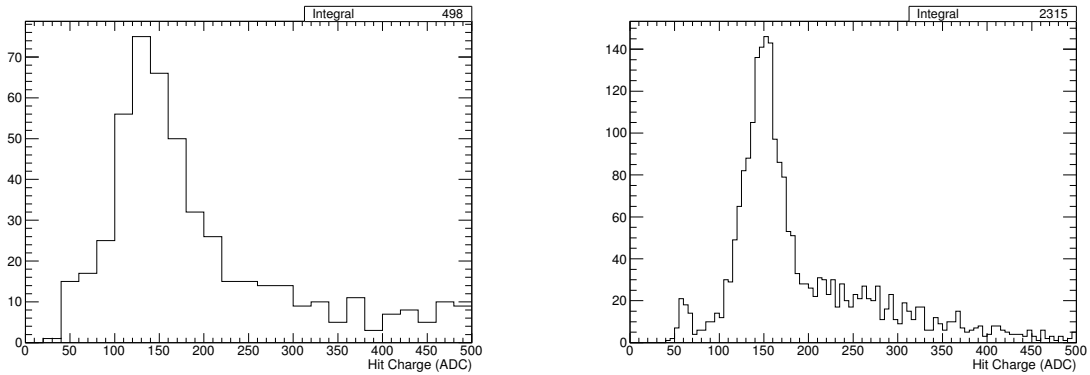


Fig. 7.22 Comparison between the distribution of T0-corrected hit times for hits on wires in front of the APA frame and away from the APA frame to validate the functionality of the mesh. Both distributions are normalised by the number of entries. There is no evidence of any differences between the two distributions so this suggests the mesh is working as intended.



(a) Hits occurring around the interaction time;  $50 < \text{tick} < 70$ . A fitted Gaussian of the peak yields a mean of 149 and a width of 49.

(b) Hits occurring away from the interaction time;  $\text{tick} < 50$ ,  $\text{tick} > 70$ . A fitted Gaussian of the peak yields a mean of 152 and a width of 28.

Fig. 7.23 Average lifetime-corrected charge per hit for hits on an APA crossing track separated according to whether or not the hit was collected around the interaction time. There is no evidence to suggest the ‘extra’ hits collected around the interaction time have significantly more or less average charge than ‘regular’ hits.

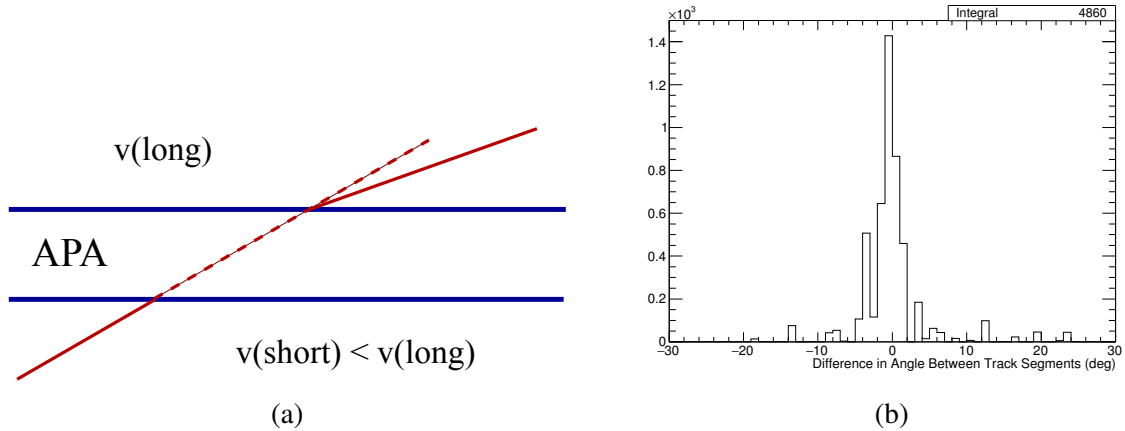


Fig. 7.24

collection plane for a given event should peak at zero if similar levels of noise were observed in each drift region; this is confirmed in Figure ??.

## 7.4 APA Gap-Crossing Muons

## 7.5 Shower Reconstruction in 35 ton Data

# **Chapter 8**

## **Electron Reconstruction for $\nu_e$ Oscillation Signal at the DUNE Far Detector**



# **Chapter 9**

## **Summary**



# References

- [1] Amerio, S., Amoruso, S., Antonello, M., Aprili, P., Armenante, M., Arneodo, F., Badertscher, A., Baiboussinov, B., Baldo Ceolin, M., Battistoni, G., Bekman, B., Benetti, P., Bernardini, E., Bischofberger, M., Borio di Tiglione, A., Brunetti, R., Bruzzone, R., Bueno, A., Calligarich, E., Campanelli, M., Carbonara, F., Carpanese, C., Cavalli, D., Cavanna, F., Cennini, P., Centro, S., Cesana, A., Chen, C., Chen, D., Chen, D. B., Chen, Y., Cid, R., Cline, D. B., Cie??lik, K., Cocco, A. G., Corti, D., Dai, Z., de Vecchi, C., Dabrowska, A., di Cicco, A., Dolfini, R., Ereditato, A., Felcini, M., Ferella, A., Ferrari, A., Ferri, F., Fiorillo, G., Galli, S., Garcia Gamez, D., Ge, Y., Gibin, D., Gigli Berzolari, A., Gil-Botella, I., Graczyk, K., Grandi, L., Guglielmi, A., He, K., Holeczek, J., Huang, X., Juszczak, C., Kielczewska, D., Kisiel, J., Kozlowski, T., Kuna-Ciskal, H., Laffranchi, M., Lagoda, J., Li, Z., Lisowski, B., Lu, F., Ma, J., Mangano, G., Mannocchi, G., Markiewicz, M., Martinez de la Ossa, A., Matthey, C., Mauri, F., Mazza, D., Melgarejo, A. J., Menegolli, A., Meng, G., Messina, M., Mietelski, J. W., Montanari, C., Muraro, S., Navas-Concha, S., Nicoletto, M., Nowak, J., Nurzia, G., Osuna, C., Otwinowski, S., Ouyang, Q., Palamara, O., Pascoli, D., Periale, L., Piano Mortari, G., Piazzoli, A., Picchi, P., Pietropaolo, F., P??lchlopek, W., Prata, M., Rancati, T., Rappoldi, A., Raselli, G. L., Rico, J., Rondio, E., Rossella, M., Rubbia, A., Rubbia, C., Sala, P., Santorelli, R., Scannicchio, D., Segreto, E., Seo, Y., Sergiampietri, F., Sobczyk, J., Spinelli, N., Stepaniak, J., Sulej, R., Szeptycka, M., Szarska, M., Terrani, M., Trinchero, G., Velotta, R., Ventura, S., Vignoli, C., Wang, H., Wang, X., Woo, J., Xu, G., Xu, Z., Yang, X., Zalewska, A., Zalipska, J., Zhang, C., Zhang, Q., Zhen, S., and Zipper, W. (2004). Design, construction and tests of the ICARUS T600 detector. *Nuclear Instruments and Methods in Physics Research, Section A: Accelerators, Spectrometers, Detectors and Associated Equipment*, 527(3):329–410.
- [2] Curioni, A., Fleming, B. T., Jaskierny, W., Kendziora, C., Krider, J., Pordes, S., Soderberg, M., Spitz, J., Tope, T., and Wongjirad, T. (2009). A regenerable filter for liquid argon purification. *Nuclear Instruments and Methods in Physics Research, Section A: Accelerators, Spectrometers, Detectors and Associated Equipment*, 605(3):306–311.
- [3] Nygren, D. R. (1974). The Time Projection Chamber - A New 4pi Detector for Charged Particles. *eConf*, C740805(PEP-0144):58–78.
- [4] Rubbia, C. (1977). The Liquid Argon Time Projection Chamber: A New Concept For Neutrino Detectors.pdf.
- [5] Tope, T., Adamowski, M., Carls, B., Hahn, A., Jaskierny, W., Jostlein, H., Kendziora, C., Lockwitz, S., Pahlka, B., Plunkett, R., Pordes, S., Rebel, B., Schmitt, R., Skup, E., Stancari, M., and Yang, T. (2014). Extreme argon purity in a large, non-evacuated cryostat. 1169(2014):1169–1175.



# **Appendix A**

## **How to install L<sup>A</sup>T<sub>E</sub>X**

### **Windows OS**

#### **TeXLive package - full version**

1. Download the TeXLive ISO (2.2GB) from  
<https://www.tug.org/texlive/>
2. Download WinCDEmu (if you don't have a virtual drive) from  
<http://wincdemu.sysprogs.org/download/>
3. To install Windows CD Emulator follow the instructions at  
<http://wincdemu.sysprogs.org/tutorials/install/>
4. Right click the iso and mount it using the WinCDEmu as shown in  
<http://wincdemu.sysprogs.org/tutorials/mount/>
5. Open your virtual drive and run setup.pl

or

#### **Basic MikTeX - T<sub>E</sub>X distribution**

1. Download Basic-MiK<sub>T</sub>E<sub>X</sub>(32bit or 64bit) from  
<http://miktex.org/download>
2. Run the installer
3. To add a new package go to Start » All Programs » MikTex » Maintenance (Admin) and choose Package Manager

4. Select or search for packages to install

## **TexStudio - T<sub>E</sub>X editor**

1. Download TexStudio from  
<http://texstudio.sourceforge.net/#downloads>
2. Run the installer

## **Mac OS X**

### **MacTeX - T<sub>E</sub>X distribution**

1. Download the file from  
<https://www.tug.org/mactex/>
2. Extract and double click to run the installer. It does the entire configuration, sit back and relax.

## **TexStudio - T<sub>E</sub>X editor**

1. Download TexStudio from  
<http://texstudio.sourceforge.net/#downloads>
2. Extract and Start

## **Unix/Linux**

### **TeXLive - T<sub>E</sub>X distribution**

#### **Getting the distribution:**

1. TeXLive can be downloaded from  
<http://www.tug.org/texlive/acquire-netinstall.html>.
2. TeXLive is provided by most operating system you can use (rpm, apt-get or yum) to get TeXLive distributions

## Installation

1. Mount the ISO file in the mnt directory

```
mount -t iso9660 -o ro,loop,noauto /your/texlive####.iso /mnt
```

2. Install wget on your OS (use rpm, apt-get or yum install)

3. Run the installer script install-tl.

```
cd /your/download/directory  
.install-tl
```

4. Enter command ‘i’ for installation

5. Post-Installation configuration:

<http://www.tug.org/texlive/doc/texlive-en/texlive-en.html#x1-320003.4.1>

6. Set the path for the directory of TexLive binaries in your .bashrc file

### For 32bit OS

For Bourne-compatible shells such as bash, and using Intel x86 GNU/Linux and a default directory setup as an example, the file to edit might be

```
edit $~/.bashrc file and add following lines  
PATH=/usr/local/texlive/2011/bin/i386-linux:$PATH;  
export PATH  
MANPATH=/usr/local/texlive/2011/texmf/doc/man:$MANPATH;  
export MANPATH  
INFOPATH=/usr/local/texlive/2011/texmf/doc/info:$INFOPATH;  
export INFOPATH
```

### For 64bit OS

```
edit $~/.bashrc file and add following lines  
PATH=/usr/local/texlive/2011/bin/x86_64-linux:$PATH;  
export PATH  
MANPATH=/usr/local/texlive/2011/texmf/doc/man:$MANPATH;  
export MANPATH
```

```
INFOPATH=/usr/local/texlive/2011/texmf/doc/info:$INFOPATH;
export INFOPATH
```

**Fedora/RedHat/CentOS:**

```
sudo yum install texlive
sudo yum install psutils
```

**SUSE:**

```
sudo zypper install texlive
```

**Debian/Ubuntu:**

```
sudo apt-get install texlive texlive-latex-extra
sudo apt-get install psutils
```

# **Appendix B**

## **Installing the CUED class file**

$\text{\LaTeX}.\text{cls}$  files can be accessed system-wide when they are placed in the  $\langle\text{texmf}\rangle/\text{tex}/\text{latex}$  directory, where  $\langle\text{texmf}\rangle$  is the root directory of the user's  $\text{\TeX}$  installation. On systems that have a local texmf tree ( $\langle\text{texmflocal}\rangle$ ), which may be named "texmf-local" or "localtexmf", it may be advisable to install packages in  $\langle\text{texmflocal}\rangle$ , rather than  $\langle\text{texmf}\rangle$  as the contents of the former, unlike that of the latter, are preserved after the  $\text{\LaTeX}$  system is reinstalled and/or upgraded.

It is recommended that the user create a subdirectory  $\langle\text{texmf}\rangle/\text{tex}/\text{latex}/\text{CUED}$  for all CUED related  $\text{\LaTeX}$  class and package files. On some  $\text{\LaTeX}$  systems, the directory look-up tables will need to be refreshed after making additions or deletions to the system files. For  $\text{\TeX}{}^{\text{Live}}$  systems this is accomplished via executing "texhash" as root. MIK $\text{\TeX}$  users can run "initexmf -u" to accomplish the same thing.

Users not willing or able to install the files system-wide can install them in their personal directories, but will then have to provide the path (full or relative) in addition to the filename when referring to them in  $\text{\LaTeX}$ .

